DESIGN AND ANALYSIS OF V-BAND ELECTROLESS PLATED TROUGH

WAVEGUIDE ANTENNA

A Thesis

by

ANOOP DILIPKUMAR TIWARI

Submitted to the Office of Graduate and Professional Studies of
Texas A&M University
in partial fulfillment of the requirements for the degree of

MASTER OF SCIENCE

Chair of Committee,	Gregory H. Huff
Co-Chair of Committee,	Robert D. Nevels
Committee Members,	Jean-Francois Chamberland
	Behbood Zoghi
Head of Department,	Miroslav M. Begovic

December 2019

Major Subject: Electrical Engineering

ABSTRACT

Design feasibility and antenna element choices make linear antenna arrays a preferred choice for applications at frequencies above 1 GHz. However, restricted bandwidth and limited scanning capabilities reduce the usefulness of these arrays in certain applications. Travelling wave antennas can overcome these problems by varying the phase velocity inside the transmission line to provide a high bandwidth scanning capability. The main beam of such a travelling wave antenna is able scan from the near-endfire to the broadside region. However, the change in the angle of the main beam from endfire to broadside introduces a high impedance mismatch which causes attenuation and reflection losses in the antenna. This research explores impedance matching techniques which could enhance the performance of beam scanning systems by solving this problem. This work covers the design, fabrication, and testing of a V-band Trough waveguide antenna (TWA) which uses tuning elements inside the guide for each perturbation. Additionally, this research covers the design and fabrication of two types of waveguide transitions. One transition connects standard rectangular waveguide to a troughguide, and another transition converts circular waveguide to a troughguide. These transitions achieve the correct orientation of modes at the input of the trough waveguide for a proper operation of the antenna.

The initial TWA design uses a rectangular base which is developed into a curved base for each channel in the final design. The curved base improves the fluid flow utilized in the fabrication process of TWA. The initial design used rectangular matching posts

attain matching and reduce the reflections at the interface of each perturbation. The final designs used circular/hemispherical matching elements with dimensions based on the rectangular posts allowed smooth edges. The author analyzed tuning elements of various shapes to obtain impedance matching while ensuring the dimensions are viable on the 3D printer available.

The next phase of the study investigated maximizing the efficiency and radiation characteristics of the antenna by maximizing the radiated power. Finally, the author attempts reduction in sidelobes of the antenna using amplitude tapering functions such as squared cosine and triangular window for the trough waveguide antenna. The resulting antenna achieves a narrow broadside beam which can be scanned for the entire V-band frequency.

ACKNOWLEDGEMENTS

CONTRIBUTORS AND FUNDING SOURCES

Contributors

This work was supervised by a thesis committee consisting of Dr. Gregory Huff and Dr. Robert Nevels as committee Chair and Co-Chair, along with Dr. Jean-Francois Chamberland of the Department of Electrical and Computer Engineering and Dr. Ben Zoghi of the Department of Engineering Technology and Industrial Distribution as committee members.

The fabrication process explained in Chapter II and Chapter III has been outlined by the members of Huff's Research Group (HRG) at the Electromagnetics and Microwave Laboratory in the Department of Electrical Engineering.

All other work conducted for the thesis was completed by the student independently.

Funding Sources

NOMENCLATURE

RWG	Rectangular Wave Guide
CWG	Circular Wave Guide
TM	Transverse Magnetic
TEM	Transverse Electromagnetic
TE	Transverse Electric
TWA	Trough Wave Antenna
LWA	Leaky Wave Antenna
TWG	Trough Wave Guide
RF	Radio Frequency
SLA	Stereolithography
3D	Three Dimensional
RP	Rapid Prototyping
CTWG	Circular Trough Wave Guide
EM	Electromagnetics
VSWR	Voltage Standing Wave Ratio

TABLE OF CONTENTS

LIST OF FIGURES

CHAPTER I

INTRODUCTION

With the increasing demand for innovative designs to meet the needs of 5G and Radar technology, it is very crucial to investigate viable options for the front-end communication systems. These systems may be Antenna arrays, receiver or transmitter designs capable to pinpoint a specific location maintaining high accuracy in data. The signal received can then be used for various applications such as Cellular connectivity with high data rate or an Autonomous vehicle trying to scan the base-stations for accurate GPS data. Anything which comes into the market must go through a rigorous testing cycle where it can be modified for all the shortcomings. Developing a proof of concept needs a technique where prototypes can be developed and manufactured within a short span of time.

Leaky Wave antennas with close structures perform well and have a closed waveguide for uniform guiding structures. At millimeter wavelengths these designs seem to have two major challenges, first is the small physical dimensions of guiding structures and the tuning mechanisms, second is the high losses incurred at such high frequencies. There is a need for having an open structure which increases the energy density and lowers the loss arises. Trough waveguide antenna proves to be a suitable choice for such requirements since leakage is controllable for a fast wave configuration. Apart from overcoming these shortcomings, trough waveguide provides a 50% increase in the operating bandwidth and frequency scanning capabilities.

1

Radiation obtained from leaky antennas have a main beam from near endfire to near broadside with an increased attenuation at broadside regions. When the beam is normal to the direction of the line, there is an impedance mismatch which occurs causing an increase in the reflection coefficient. This research targets to solve this problem using some tuning mechanism at the interface of periodic discontinuity. The gain of the antenna can be increased with the increase in the number of unit cells, but there is sharp rise in the reflection loss. To reduce this reflection and convert more energy into the TEM mode, tuning posts of required height and width can be utilized. The reflections occurring at each interface appears as a shunt negative susceptance which can be matched with capacitive tuning posts. Previous work has been done in this area where the tuning posts have been added to the septum. But designing TWA at a frequency of 60Ghz has a limit on the thickness of septum and adding tuning posts is not feasible. An attempt has been made in this research to create tuning posts on the side walls of the TWG and modifying the design to enable rapid prototyping using additive manufacturing techniques.

A Circular Waveguide to Circular Trough Waveguide and a Rectangular Waveguide to Circular Trough Waveguide transition has been designed to convert the dominant mode into troughguide mode. Back to back configuration with a small length of trough waveguide is fabricated and the results have been discussed in chapter III. Once the mode conversion has been established, the Trough waveguide antenna is analyzed for design modifications and impedance matching. The Trough waveguide having rectangular base and rectangular perturbations have been studied in comparison with the modified design. The matching techniques used for reduction in reflections from the perturbations

2

has been done with a simple rectangular post and a spherical tuning post as well. Antipodal perturbations matched using spherical matching posts has been designed and fabricated discussed in Chapter IV. The designed antenna with matching is capable of frequency scanning applications. This design is then used as a single unit element for creating an array to study the overall gain of the system and beam scanning capabilities of Trough Waveguide array.

CHAPTER II

BACKGROUND

II.1 Waveguides

Waveguides serve as a means for propagating electromagnetic energy at high frequencies with very low loss as compared to other lossy transmission lines. These are a hollow tube with one conductor used as a transmission lines for transmitting waves in a communication system. The inner walls of the tube provide a distributed inductance and the empty space provide a distributed capacitance. Using this understanding, the model for waveguide as a transmission line has been developed. The cross-sectional dimension of the waveguide determines various frequency bands for which it can be used. These structures may be rectangular, or circular as shown in Figure 1 based on the orientation of the field components inside the structure.
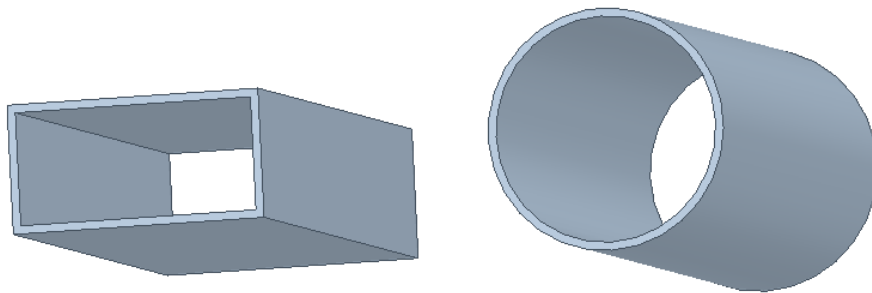
Figure 1: Rectangular and Circular waveguides.

If we consider a time-harmonic electromagnetic wave propagating along the +z axis inside a rectangular waveguide, the electric and magnetic fields are transverse to the direction of propagation and transverse to each other. The orientation of either E field or

H field depends on the mode traveling into the waveguide. One of the fields is traveling and the other one loops around being perpendicular to each other and to the direction of wave propagation. Considering the time-harmonic form of Maxwell's equations for a source free transmission line, we can derive the vector components for respective fields.

$$\nabla \times \bar{E} = -jw\mu\bar{H} \tag{1}$$

$$\nabla \times \bar{H} = j\omega\varepsilon\bar{E} \tag{2}$$

The three vector components (x, y, z) of E and H field can then be reduced into the equations (3)-(8). Where β is the phase constant, and it is replaced by the propagation constant gamma ($\gamma = \alpha + j\beta$) when including both the conductor and dielectric losses represented by α. The transverse field components can then be applied to different types of waveguide systems with a mode orientation pertaining to the required operation.

$$\frac{\partial E_2}{\partial y} = j\beta E_2 = -j\omega\mu H_x \tag{3}$$

$$j\beta E_1 - \frac{\partial E_z}{\partial x} = -j\omega u H_y \tag{4}$$

$$\frac{\partial E_y}{\partial x} - \frac{\partial E_x}{\partial y} = -j\omega\mu H_z \tag{5}$$

$$\frac{\partial H_z}{\partial y} + j\beta H_y = j\omega\varepsilon E_x \tag{6}$$

$$-j\beta H_x - \frac{\partial H_2}{\partial x} = j\omega\varepsilon E_y \tag{7}$$

$$\frac{\partial H_y}{\partial x} - \frac{\partial H_x}{\partial y} = j\omega\varepsilon E_z \tag{8}$$

II.1.1 Modes in Waveguides

Waveguides serve as the guiding structures for various designs of a leaky wave antenna. The trough waveguide antenna requires a transition from RWG or CWG to the Troughguide mode. Therefore, it becomes important to investigate the principal modes of rectangular and circular waveguides.

II.1.2 TEM mode

Transverse electromagnetic waves can exist only when two or more conductors are present in a transmission line. E_z and H_z field components are zero since the wave has no field variation along the direction of propagation. A closed waveguide cannot support TEM mode considering the static potential inside such conductor would be zero or constant. TWA being an open waveguide structure with an E field bifurcation supports the TEM mode. The wave impedance for a TEM mode can be calculated using the transverse E and H field components. Equation x can be combined with the other two vector field components to give a general equation of the transverse field denoted by $\overline{h}(x,y)$. η is the free space wave impedance.

$$z_{TEM} = \frac{E_x}{H_y} = \frac{-E_y}{H_x} = \frac{\omega\mu}{\beta} = \sqrt{\frac{\mu}{\varepsilon}} = \eta \tag{9}$$

$$\overline{h}(x,y) = \frac{1}{z_{1EM}} \hat{z}_x \overline{e}(x,y) \tag{10}$$

II.1.3 TE10 mode in RWG
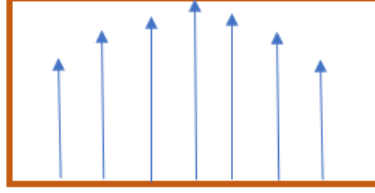
Figure 2: TE10 E-fields in RWG.

For a rectangular waveguide placed along the x-axis, the propagation constant is given by equation (11), where k is known as free space wave number, k_c as the cutoff wave number. a and b are the dimensions for broad and narrow walls of the waveguide respectively and m and n are the mode combinations.

$$\beta = \sqrt{k^2 - k_c^2} = \sqrt{k^2 - \left(\frac{m\pi}{a}\right)^2 - \left(\frac{n\pi}{b}\right)^2} \tag{11}$$

The general equation for calulating the cutoff frequecny of certain mode propagation is given by $f_{c_{mn}}$ [2]. Calculating the lowest cutoff frequency i.e TE10 mode we substitute $m = 1$ and $n = 0$.

$$f_{c_{mn}} = \frac{k_c}{2\pi\sqrt{\mu\varepsilon}} = \frac{1}{2\pi\sqrt{\mu\varepsilon}}\sqrt{\left(\frac{m\pi}{a}\right)^2 + \left(\frac{n\pi}{b}\right)^2}, \; f_{c_{10}} = \frac{1}{2a\sqrt{\mu\varepsilon}} \tag{12}$$

Wave impedance is given by the transverse field components,

$$z_{TE} = \frac{E_x}{H_y} = \frac{-E_y}{H_x} = \frac{k\eta}{\beta} \tag{13}$$

7

The wavelength between two equi-phase planes is know as guide wavelength, greater than the free space wavelength. And v_p is the phase velocity which is greater than the speed of light.

$$\lambda_g = \frac{2\pi}{\beta} > \frac{2\pi}{k} = \lambda \tag{14}$$

$$v_p = \frac{\omega}{\beta} > \frac{\omega}{k} = \frac{1}{\sqrt{\mu\varepsilon}} \tag{15}$$

II.1.4 TE11 CWG
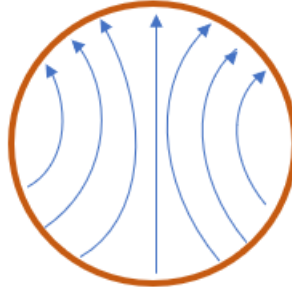
Figure 3: TE11 mode E-fields in CWG.

Similarly using the vector equations of circular waveguide, TE11 mode can be calculated. The wave impedance and the cutoff wavelength can be computed using the following equations, where P'_{mn} is a constant dependent on the mode and a is the radius of the waveguide cross section. Figure 3 shows the E-fields inside the waveguide.

$$k = \omega\mu\varepsilon \tag{16}$$

$$k_c = \frac{P'_{mn}}{a} \tag{17}$$

$$z = z_{TE} = \frac{kn}{\rho} \tag{18}$$

II.2 Traveling Wave Antennas

Traveling wave antennas are classified into the antennas that utilize wave travelling on a guiding structure for generating radiation. It is defined as antennas for which currents on the guiding structure and fields generated inside and around the guide producing the pattern represented by many traveling waves ideally in the same direction [3]. The mode propagating on the transmission line and the terminations used, create a traveling wave current and field distribution. Long slots in waveguides, helical antennas, long wire and rhombic antennas are some of the examples of traveling wave antenna.

Consider a line source with a sinusoidal time variation having a complex current distribution given by equation (19) with amplitude and phase components.

$$I(z) = |I(z)|e^{-j\psi(2)} \tag{19}$$

If each wave has a constant amplitude and uniform phase velocities, it can be represented as a sum of all waves given in equation (20).

$$I(z) = \sum_n A_n e^{-j\beta_n z} \tag{20}$$

The traveling wave will have some attenuation, therefore I(z) can be represented using equation (21) as damped waves.

$$I(z) = \sum_n B_D e^{-\gamma_n z} \tag{21}$$

Traveling wave antennas are categorized into slow and fast Wave antennas depending on the phase velocity of the propagating wave. Phase velocity is defined the ratio of angular frequency omega and phase constant beta,

$$v_p = \frac{\omega}{\beta} \tag{22}$$

9

II.2.1 Surface wave Antenna

If the phase velocity is less than the speed of plane wave in free space, then it is known as Slow wave ($\frac{c}{v} > 1$) referred as surface wave. Fundamentally these waves do not radiate, but radiation occurs only at discontinuities such as terminations and the feed. Highly directive beam is difficult to obtain since the overall radiation is caused by multiple sources on the structure. A moderately-directive pattern can be obtained near endfire area with a main beam having significant sidelobe.

II.2.2 Leaky Wave Antennas

If the phase velocity of a traveling wave is greater than the speed of plane wave in free space it is known as Fast wave ($\frac{c}{v} < 1$), usually referred as Leaky waves. A continuous radiation is caused by the such a wave along the length, having the propagation wavenumber k_z consisting of both a phase and an attenuation constant [4]. Highly-directive beams can be achieved at an arbitrary specified angle with this type of antenna, having a low sidelobe level. The beam angle is controlled by the phase constant β, while the Beamwidth is controlled by the attenuation constant α. Overall beam shape can be controlled by tapering the aperture distribution of the radiating structure.

Leaky-wave antennas can be divided into two important sections, uniform and periodic, based on the operation and geometry of the guide structure. The following sections describes the various configurations of the Leaky-wave antenna in brief.
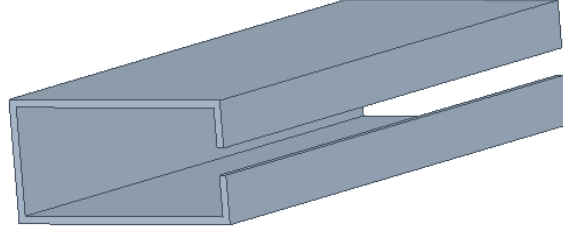
II.2.3 Uniform Leaky Wave Antenna

Figure 4: Longitudinal slot in RWG.

The cross section of the structure along the length is uniform, it can be a waveguide with a longitudinal slot on one side as shown in Figure 4. It enables the guiding wave to radiate energy continuously as it is traveling. This type of LWA has propagates fast wave for the dominant mode and can scan from near endfire to near broadside regions. We take example of an air-filled longitudinal slot waveguide with dominant TE10 mode (fast wave) and phase constant beta equation here. Using the stationary phase theory, angle of maximum radiation for broadside is given by equation (23).

$$\frac{\beta}{k_0} = \frac{c}{v} = \frac{\lambda_0}{\lambda_g} \approx \sin \theta_m \qquad (23)$$

For a length of guide L and a small value of alpha, a narrow beam having a half power beamwidth of $\Delta\theta$ can be obtained.

$$\Delta\theta \cong \frac{1}{\frac{L}{\lambda_0} \cos \theta_m} \qquad (24)$$

And for a waveguide radiating 90% of the power following relation can be utilized:

$$\frac{L}{\lambda_0} \approx \frac{0.18}{\frac{\alpha}{k_0}} \Rightarrow \Delta\theta \propto \frac{\alpha}{k_0} \qquad (25)$$

A small alpha constitutes to a large aperture and a large value of alpha conversely results into a smaller aperture. The radiation efficiency is dependent on the length of

11

waveguide and an optimum length must be considered so that maximum power is radiated with fields diminishing at the end of the slit. The side lobes of the radiation pattern can be reduced by applying a taper to the physical geometry of the structure as the wave decays exponentially.

II.2.4 Periodic Leaky Wave Antenna
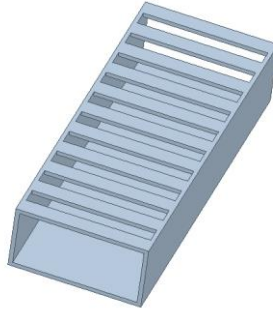
Figure 5: Periodic slots in RWG.

Periodic LWA consists of some discontinuities used to modulate the wave periodically by creating alterations in the guiding structure, shown in Figure 5. This structure supports a slow wave being radiated continuously along the length. The beamwidth and radiation efficiency of Leaky wave antennas can be controlled with the value of alpha and beta of the complex propagation constant same as that for Uniform LWA.

Since it supports slow wave propagation, it does not radiate energy from the open end. So, in order to make the wave radiate, one of the infinite space harmonics is made to be fast space(*n=-1*). The radiation characteristics of Periodic LWA is from Backward endfire to broadside with an open stop band around exact broadside.

$$cos\,\theta_m \approx \frac{k_t}{k_0} = \Delta\theta \approx \frac{2\pi}{k_t L} = \frac{\lambda_c}{L} \tag{26}$$

12

II.3 Trough Waveguide Antenna

The design and properties of Trough Waveguide (TWG) have been studied by Rotman and Oliner [5] using various techniques for phase accumulation. The guide wavelength has been varied changing the phase velocity to create slow and fast waves inside the trough waveguide [6]. Trough waveguide has been derived from the strip transmission line with dominant TE01 mode, where the structure is divided in two parts at the center as shown in Figure 6. The resulting structure with a center septum called as the trough waveguide having TE01 and TEM mode appears as shown in figure 7.
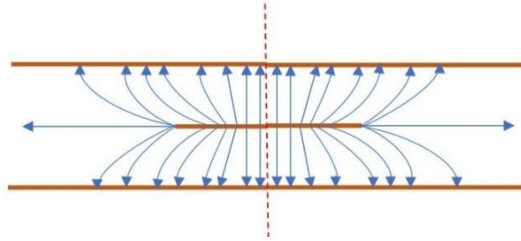
Figure 6: Strip Transmission line with TE01 Mode.
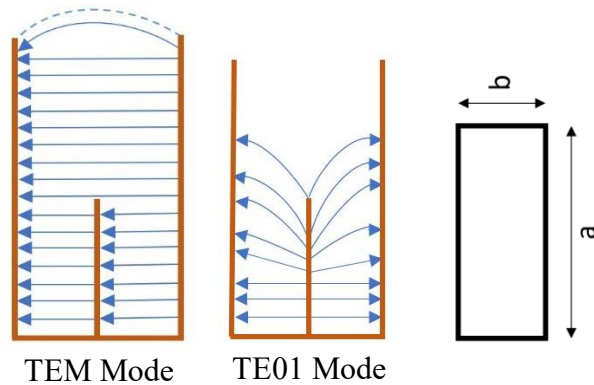

TEM Mode   TE01 Mode

Figure 7: Trough waveguide with TE01 Mode and equivalent RWG.

The septum divides the waveguide into two symmetric sections each having same field configuration. It can also be viewed as two rectangular waveguides placed side by

side with one of the broad walls in contact with each other placed vertically to form two channels. This structure is a non-radiating line whose cut-off and guide wavelength (λg) are determined by the equation 27, where λo is the operating free space wavelength.

$$\lambda_c = \frac{\lambda_0}{\sqrt{1 - \left[\frac{\lambda_0}{\lambda g}\right]^2}} \tag{27}$$

The cutoff wavelength (λ_c) depends on the dimension of the Trough waveguide septum and a small offset value (δ) added due to the height of the magnetic wall above the septum as shown in figure 8.

$$s + \delta = \lambda c \, / \, 4 \tag{28}$$
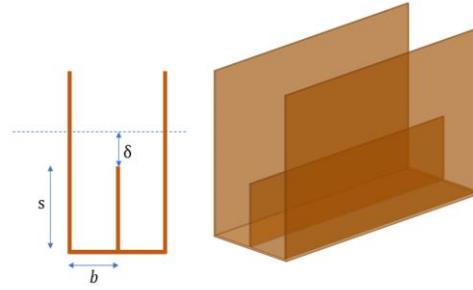
Figure 8: Trough waveguide with 3D Model with dimensions.

This line can be made radiating when an asymmetry is introduced either side of the TWG [3]. Aperiodic or continuous asymmetry shown in figure 9 is introduced to attain an endfire/near-endfire radiation [7]. This is achieved by increasing the base height on either side which allows us to control the phase velocity with a beam emerging at an angle given by equation (29). This line can be viewed as a lossy transmission line where TE01 mode is coupled into TEM mode on the two side walls away from the septum.

$$\sin \theta = \frac{\lambda_0}{\lambda g} \tag{29}$$

14
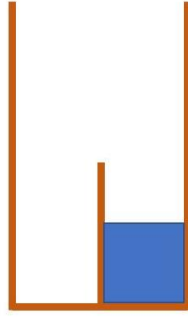
Figure 9: Trough waveguide with one side having continuous asymmetry.

Broadside beam can only be achieved when the guide wavelength is infinite, which restricts the beam at an angle given in equation (29). A phase reversal of 180 degrees is required to attain a broadside or near-broadside beam. This is achieved by alternately placing blocks half-wavelength in length on each side of the TWG as show in fig 10.

Figure 10: Trough waveguide with alternate blocks on each side. (Unit Cell)

A broadside beam emerges which can be frequency scanned keeping the length same or it can be scanned changing the length of the blocks (L). This antenna is known as periodically asymmetric trough waveguide, where angle of the principal maxima is given by equation (30).

$$\sin \theta = \frac{\lambda_0}{\lambda g} - \frac{\lambda_0}{2L} \qquad (30)$$

15

II.4 S-parameter

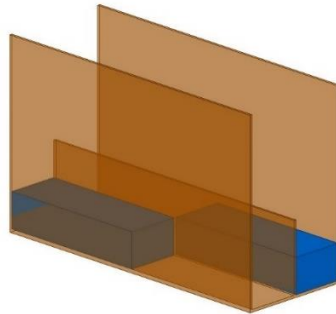S-parameters are defined based on waves with constant amplitude traveling on a lossless transmission line. The traveling wave component contrasts with the varying RF voltages and current conventionally used to define Y and Z matrix. This characteristic facilitates the effective measurement of RF circuits since it can be performed by an appropriate instrument such as a vector network analyzer at locations away from the circuits, provided that low loss transmission lines (ideally lossless transmission lines) are used in between.
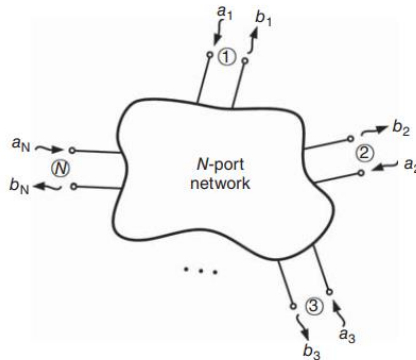

Figure 11: N-port network.

Consider a N-port network similar to Figure 11, with a terminating transmission line having characteristic impedance of Zo to be lossless. The input and output terms, a's and b's are the normalized incident and reflected voltages and can be represented in a matrix form as $[b] = [S][a]$ expanded into all the s parameters as below.

$$
\begin{bmatrix} b_1 \\ b_2 \\ \vdots \\ b_N \end{bmatrix} = \begin{bmatrix} S_{11} & S_{12} & \cdots & S_{1N} \\ S_{21} & S_{22} & \cdots & S_{2N} \\ \vdots & \vdots & \cdots & \vdots \\ S_{N1} & S_{N2} & \cdots & S_{NN} \end{bmatrix} \begin{bmatrix} a_1 \\ a_2 \\ \vdots \\ a_N \end{bmatrix}
$$

The S-parameters of the N-port network can be defined using the following equations.

$$
s_{ij} = \left. \frac{b_i}{a_i} \right|_{a_{k \approx 0}(k \neq i)} \qquad s_{ij} = \left. \frac{b_j}{a_j} \right|_{a_{k \approx 0}(k \neq j)} \tag{31}
$$

We will consider a two-port network in Figure 12 for the ease of understanding the concept of S-parameters. The input to the network is given by a source having an internal impedance of Z_s with input reflection coefficient in terms of a_1 and b_1. The load impedance is Z_l with output reflection coefficient in terms of a_2 and b_2.
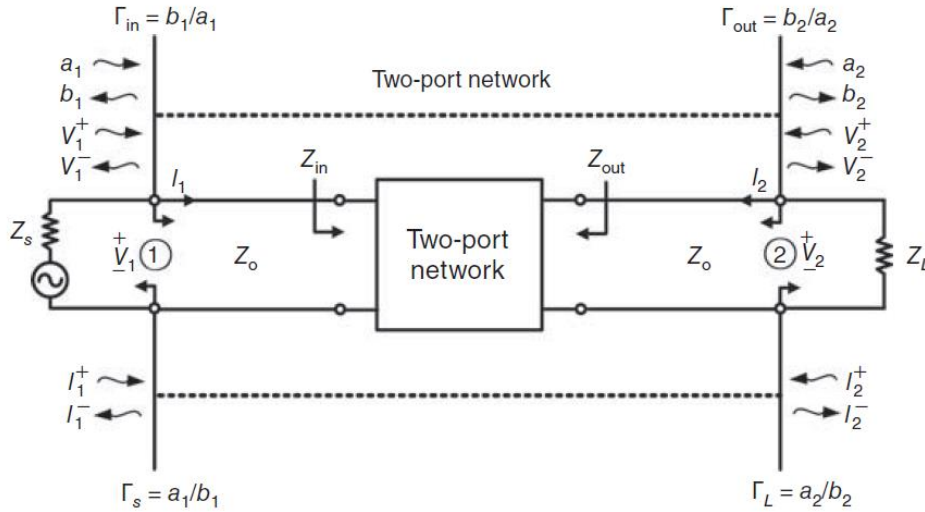

Figure 12: Two port network for S-parameter analysis.

As shown in figure the wave components of voltage and current travel in the opposite direction and the total is given by sum of forward and reverse travelling voltage and current components in terms of equations (32)-(35).

$$V_1 = V_1^+ + V_1^- \tag{32}$$

$$V_2 = V_2^+ + V_2^- \tag{33}$$

$$I_1 = I_1^+ + I_1^- = \frac{1}{Z_0}(V_1^+ - V_1^-) \tag{34}$$

$$I_2 = I_2^+ + I_2^- = \frac{1}{Z_0}(V_2^+ - V_2^-) \tag{35}$$

Based on the equivalent equations having the characteristic impedance Zo we can write the current equations in terms of voltages.

$$V_1^- = S_{11}V_1^+ + S_{12}V_2^+ \tag{36}$$

$$V_2^- = S_{21}V_1^+ + S_{22}V_2^+ \tag{37}$$

Using the normalized incident and reflected voltages at port 1 and 2, we can define the S-parameters in terms of a_1, a_2, b_1, b_2 given in equations (38) and (39).

$$b_1 = S_{11}a_1 + S_{12}a_2 \tag{38}$$

$$b_2 = S_{21}a_1 + S_{22}a_2 \tag{39}$$

For a perfectly matched port 1 and 2, We can define few important parameters in terms of incident and reflected rms power useful in evaluating the performance of passive networks.

$$|S_{11}|^2 = \frac{|b_1|^2}{|a_1|^2} = \frac{\text{Reflected power at port 1}}{\text{Incident power at port 1}} = \text{Return loss at port 1} \tag{40}$$

$$|S_{12}|^2 = \frac{|b_1|^2}{|a_2|^2} = \frac{\text{Reflected power at port 1}}{\text{Incident power at port 2}} =$$

Insertion loss from port 2 to port 1 or isolation $\hspace{2cm}$ (41)

$$|S_{21}|^2 = \frac{|b_2|^2}{|a_1|^2} = \frac{\text{Reflected power at port 2}}{\text{Incident power at port 1}} =$$

Insertion loss from port 1 to port 2 or isolation $\hspace{4cm}$ (42)

$$|S_{22}|^2 = \frac{|b_2|^2}{|a_2|^2} = \frac{\text{Reflected power at port 2}}{\text{Incident power at port 2}} = \text{ Return loss at port 2} \hspace{2cm} (43)$$

Input and output reflection coefficient are calculated in terms of the s parameters for a transmission line, given by the following equations.

$$\Gamma_{in} = s_{11} + \frac{s_{12}s_{21}\Gamma_L}{1 - s_{22}\Gamma_L} \hspace{2cm} \Gamma_{in} = S_{11} \text{ (for a matched termination)} \hspace{1cm} (44)$$

$$\Gamma_{out} = s_{22} + \frac{s_{12}s_{21}\Gamma_L}{1 - s_{11}\Gamma_L} \hspace{2cm} \Gamma_{out} = S_{22} \text{ (for a matched termination)} \hspace{1cm} (45)$$

Reflections are inevitable and there are losses occurring in a circuit, we can use return loss to characterize the matching conditions of the circuit. $RL_1 = 20\,log|\Gamma_1|(dB)$ for general termination and $RL_1 = 20\,log|S_{11}|(dB)$ for matched termination. Similarly, losses incurred due to power dissipation or radiation can be characterized in terms of insertion loss $IL_{21} = 20\,log|S_{21}|(dB)$ for matched termination. S-parameters prove to be useful in measuring the network characteristics for a simulated and a fabricated designs to arrive at a comparitive understanding of the network.

II.5 ABCD Matrix

While characterizing RF networks with arbitrary number of ports and various interconnections between ports, another Matrix commonly used is the chain matrix represented in terms of ABCD parameters. The input voltage and current terms are given in terms of the output voltage and current terms with parameters given in equation (46).

$$V_1 = AV_2 + BI_2 \tag{46}$$

$$I_1 = CV_2 + DI_2 \tag{47}$$

While working with two port networks as shown in figure 12, we come across cascade interconnections where the same output current is flowing into the second network. The overall circuit can be calculated as a multiplication between the two matrices for each network respectively. This helps in analyzing complicated microwave networks and reduce the number of network blocks into smaller equivalent network.

$$\begin{bmatrix} V_1 \\ I_1 \end{bmatrix} = \begin{bmatrix} A & B \\ C & D \end{bmatrix} \begin{bmatrix} V_2 \\ I_2 \end{bmatrix} \tag{48}$$

$$\begin{bmatrix} V_1 \\ I_1 \end{bmatrix} = \begin{bmatrix} A_1 & B_1 \\ C_1 & D_1 \end{bmatrix} \begin{bmatrix} V_2 \\ I_2 \end{bmatrix} \tag{49}$$

$$\begin{bmatrix} V_2 \\ I_2 \end{bmatrix} = \begin{bmatrix} A_2 & B_2 \\ C_2 & D_2 \end{bmatrix} \begin{bmatrix} V_3 \\ I_3 \end{bmatrix} \tag{50}$$

$$\begin{bmatrix} V_2 \\ I_2 \end{bmatrix} = \begin{bmatrix} A_1 & B_1 \\ C_1 & D_1 \end{bmatrix} \begin{bmatrix} A_2 & B_2 \\ C_2 & D_2 \end{bmatrix} \begin{bmatrix} V_3 \\ I_3 \end{bmatrix} \tag{51}$$

The two cascaded networks may appear as impedances connected in shunt and series creating circuits know as pi or T networks which are interchangeable with ABCD parameters in terms of impedance and admittance shown in Figure 13 and 14.
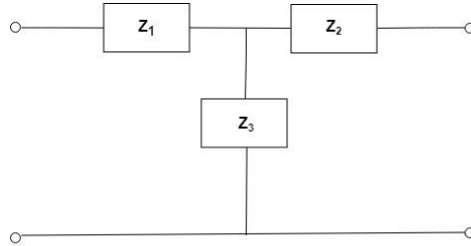

Figure 13: T-model.

$$A = 1 + \frac{Z_1}{Z_3} \qquad B = Z_1 + Z_2 + \frac{Z_1 Z_2}{Z_3} \tag{52}$$
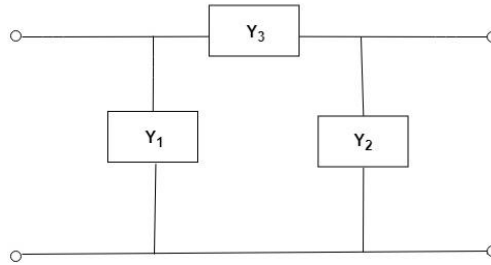
$$C = \frac{1}{Z_3} \qquad D = 1 + \frac{Z_2}{Z_3} \tag{53}$$

Figure 14: Pi-Model.

$$A = 1 + \frac{Y_2}{Y_3} \qquad\qquad B = \frac{1}{Y_3} \tag{54}$$

$$C = Y_1 + Y_2 + \frac{Y_1 Y_2}{Y_3} \qquad D = 1 + \frac{Y_1}{Y_3} \tag{55}$$

It is useful in solving the equivalent circuits of waveguides having a post placed inside which may be perpendicular or parallel to the E field.

II.6 Fabrication Techniques

Many research Labs and companies utilize a rapid prototyping technique that can create a prototype model which gives results close to the expected values. These prototyping techniques consider the fabrication errors and other known issues to predict the working and functionality for a device being considered. One such method used by the RF industries and research groups is 3D printing using additive manufacturing techniques [9]-[11]. Researchers and Engineers are combining techniques from various fields to develop a complete process. It can be a plating technique from chemical engineering or CAD modelling from mechanical design.

This research utilizes such techniques in prototyping various microwave components required for fabricating Trough waveguide antenna. These components may be individual building blocks connected to form a complete system or it can be a modular component on its own. 3D printing has been used in academic research for creating parts and interconnects with a specific design intricacy. Two step approach is being used for the complete fabrication of components, first is the 3D printing using Stereolithography (SLA) and Second is the Electroless plating of printed model for metalizing the inner and outer surface of the device.

II.6.1 Modeling

The CAD model for a microwave component is made using a modelling tool or it can be exported from any 3D EM modeler. The design should be made considering the resolution and accuracy of the printer. Once the desired results are obtained from the simulations, the CAD file is created having all the required flanges and interconnects.
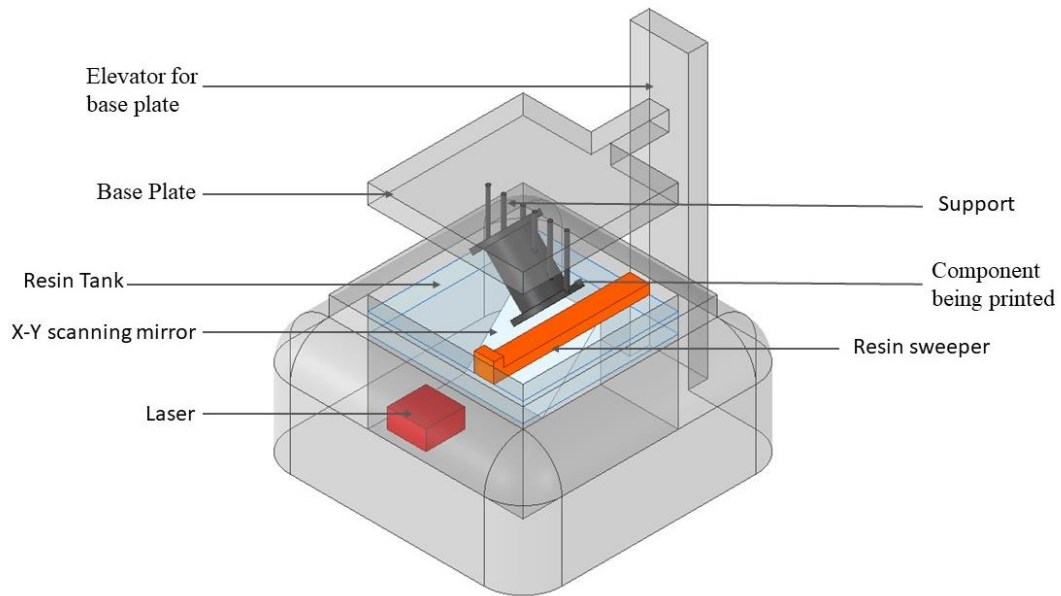
II.6.2 Printing

Figure 15: SLA Printer Technology.

Inverted SLA is one of the additive manufacturing processes that uses photosensitive resin and the method of photopolymerization for curing the materials into solid parts. The light source cures the additive manufactured resin layer by layer to convert it into a complete solid model. A resolution of 25 microns can be achieved for the structures which is highly desirable for building microwave components at a higher frequency. Once the solid structure is printed completely, the access resin sticking to the model is rinsed with isopropyl alcohol. The model is kept for UV curing to increase the strength of carbon bonds created during the printing process. Figure 15 explains the various parts utilized by the 3D printer.
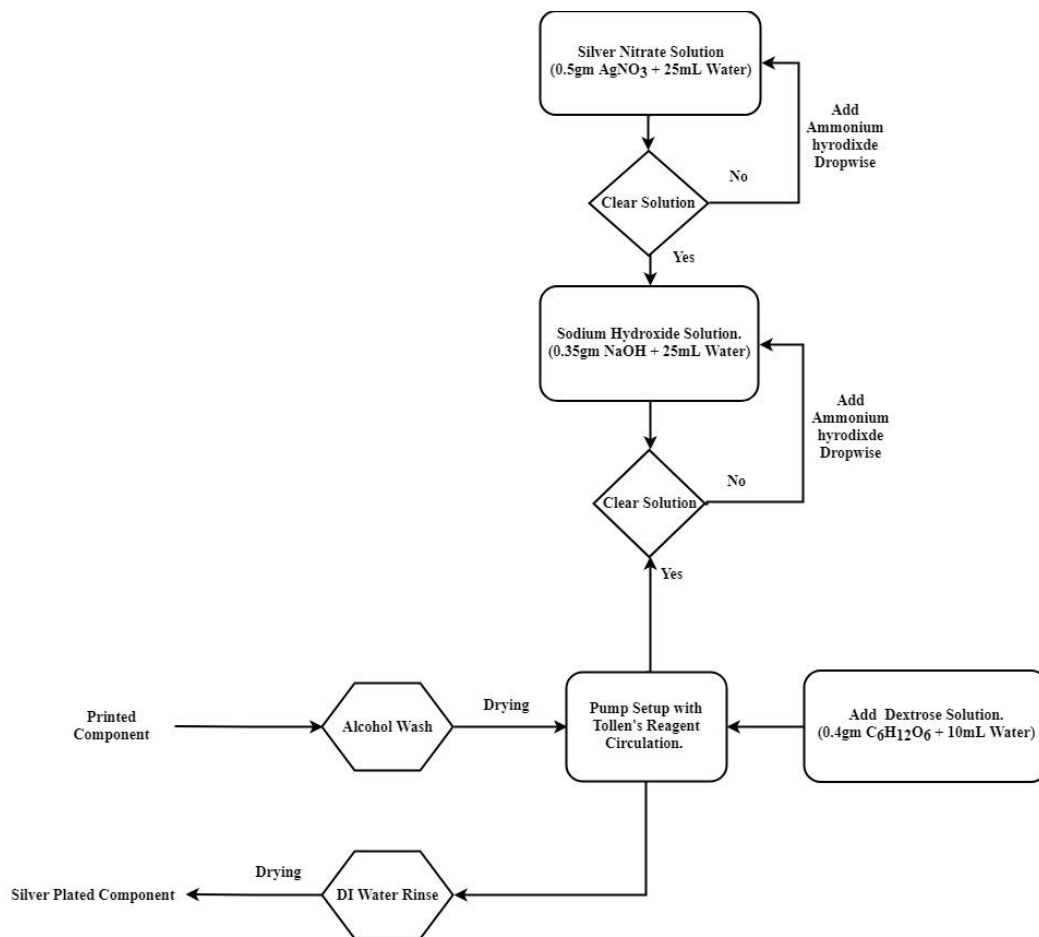
II.6.3 Plating

Figure 16: Electroless silver plating flow-chart.

Electroless silver plating is used for converting the non-conductive structures into a conductive passive microwave component. The process uses Tollens reagent and dextrose solution for plating the required surface of the components [12].
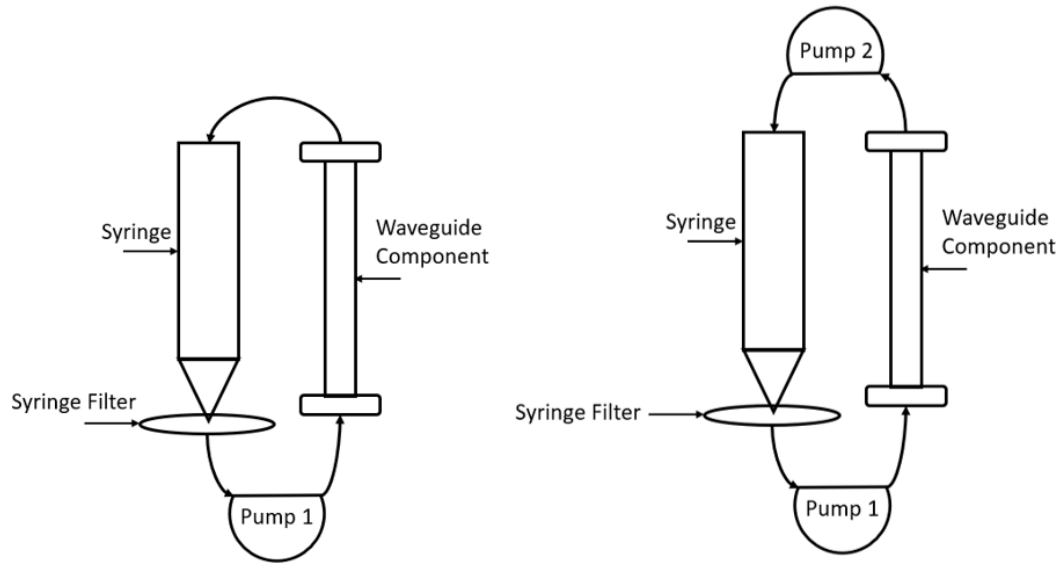
Figure 17: Peristaltic pump configuration.

The solution is pumped using a peristaltic pump connected to a syringe filter for removing the residue generated during the chemical reaction. A submicron layer of silver is deposited on the surface enabling conduction and desired operation of the component. Depending on the length and the inner surface area of the component to be plated, two pump configurations has been devised in Figure 17. First setup uses one pump to push the fluid inside the component and the second setup uses a push-pull mechanism which helps in a uniform coating of metal. The inlet and outlet of the component can be swapped for few cycles of metallization.

CHAPTER III

TROUGH WAVEGUIDE TRANSITION

III.1 Introduction

TWAs can be utilized for plasma generation or as an antenna, depending on the suitable application and feeding mechanism. Coaxial feed [13] or rectangular waveguide feed can be used along with a transition between the RWG and the TWG [14]. The RWG/CWG mode to CTWG mode conversion and impedance transformation is required for proper operation of the antenna. The septum divides the troughguide into two sections having symmetric field orientation. For a transition, the length of the tapering septum and the gradation in its height determines the impedance value and mode orientation inside the transition given in Figure 18.
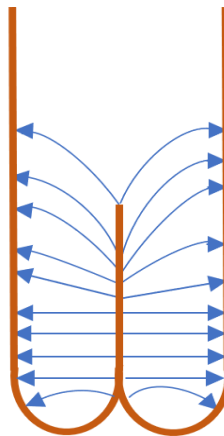

Figure 18: TWG with TE10 mode or TWG mode.

The TWA can also be connected to a beam forming network built using either rectangular or circular waveguide hybrid couplers and phase shifters. It is therefore

important to investigate the design of transitions for ensuring that correct mode excitation takes place in the CTWG. Two configurations of the transition have been considered, one is the RWG to CTWG and another is the CWG to CTWG. The design of the waveguide has been modified to support the fluid flow during the metallization process. The two channels of the rectangular TWG has been curved in a circular shape as shown in figure 18 called as Circular TWG (CTWG). The transitions have been designed with these considerations enabling laminar flow of Tollen's reagent on the surface for depositing a thin layer of silver. The first section of this chapter describes the design analysis and the operation of each cascade sections forming the transition. The second section shows the analysis for the optimum length of transitions. Based on the simulated and fabricated designs a comparative study has been done in the third section on the simulated and measured results.

III.2 Design Considerations

The design of transition includes various cutoff frequencies for the independent operation of waveguide structures. The troughguide designed has a lower cutoff frequency compared to the cutoff frequency of V-band RWG and CWG. The height of the septum is important in determining the cutoff frequency of TWG. Also, a finite thickness increases the cut-off wavelength and decreases the guide wavelength [14]. These variations have been considered and an analysis is presented for a sweep of septum height and thickness values.

27

For a fixed base dimension and finite thickness, the cutoff frequency can be estimated by $\lambda_c/4 = s + \delta$ and the value of delta can be approximated by $\delta = \frac{2b}{\pi} ln\, 2$. The simulation results are close to the calculated values shown on the right side of following plots.
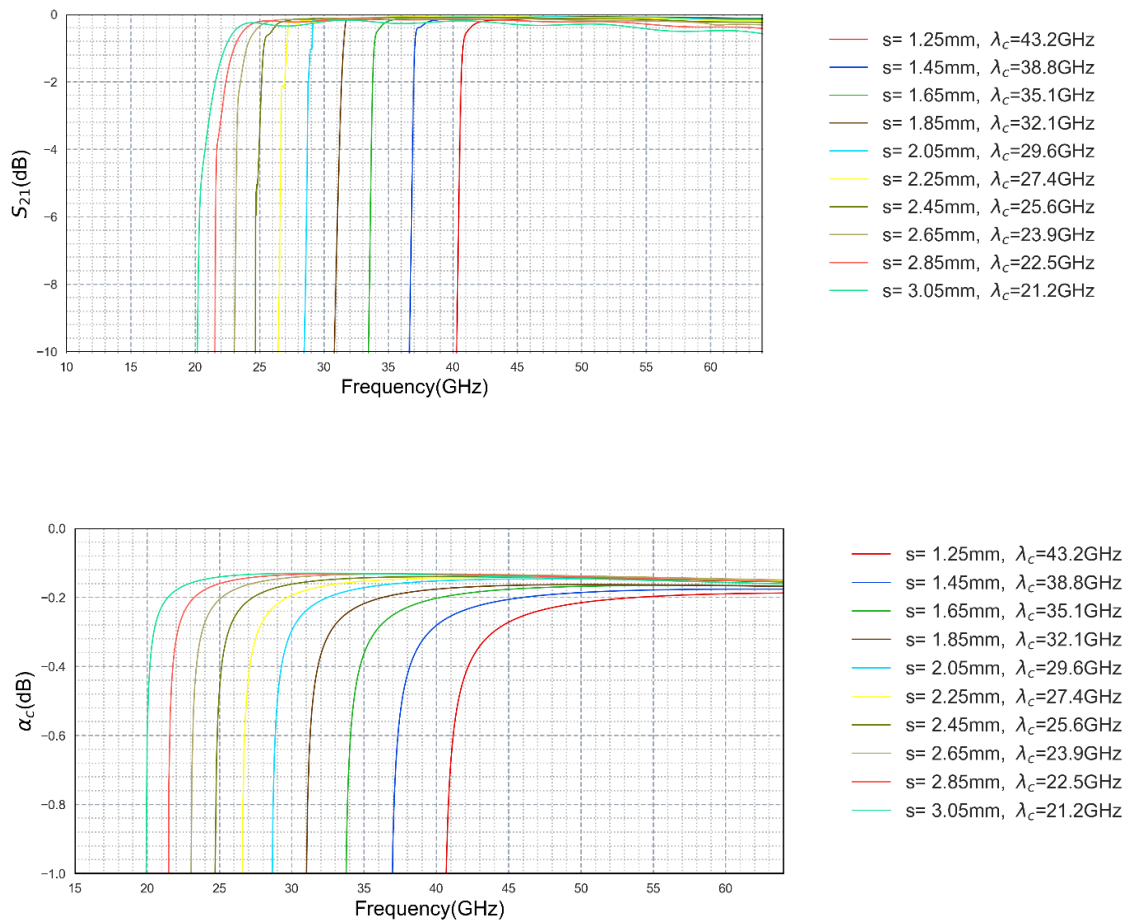

Figure 19: Variation in Cutoff frequency with changes in septum height.

Figure 19 and 20 show the insertion loss and attenuation inside the waveguide for variation in septum height. The magnetic wall above the septum moves up when the height of the septum is increased, this causes a change in the cutoff wavelength.
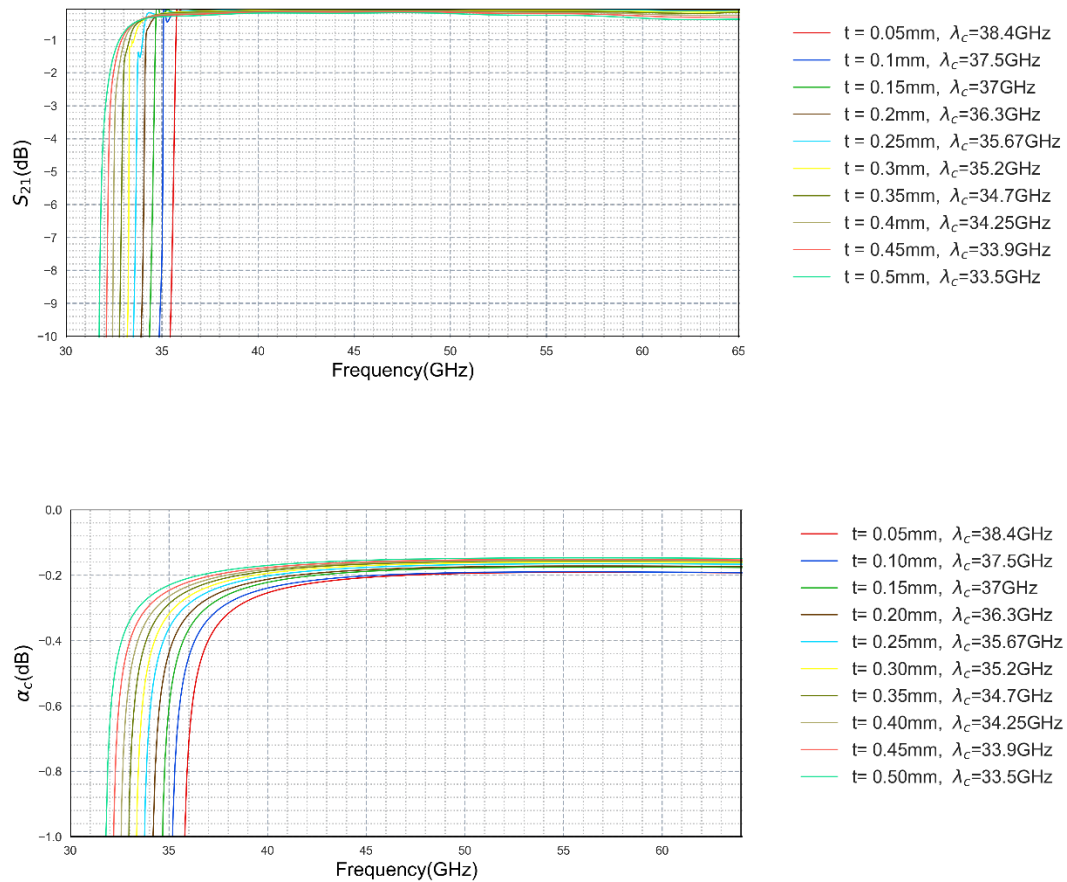
Figure 20: Variation in Cutoff frequency with changes in septum thickness.

The dimensions of WR-15 rectangular waveguide with broad wall a_2 and narrow wall b_2 is used on one side and a CTWG having horizontal width b_1 and vertical height a_1 is used on the other side. The base of the CTWG is made of two cylindrical surfaces having a diameter b separated by a septum of thickness t ($b_1 = 2b + t$). This thickness of the septum

29

is uniform throughout the transition and the troughguide. The transition is of length L with the septum height in gradation from value to s. The side walls of the transition flares in to the troughguide with the base on the same plane. The top and bottom walls become narrow to match the horizontal dimension b_1 of the troughguide.
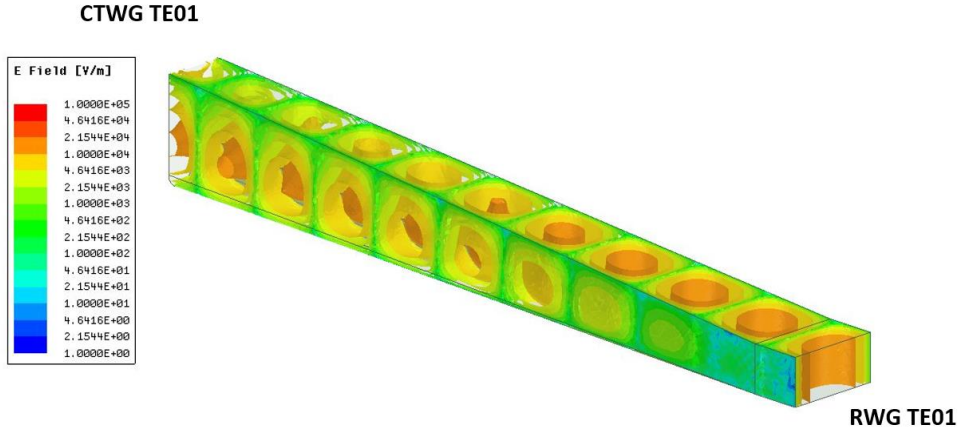

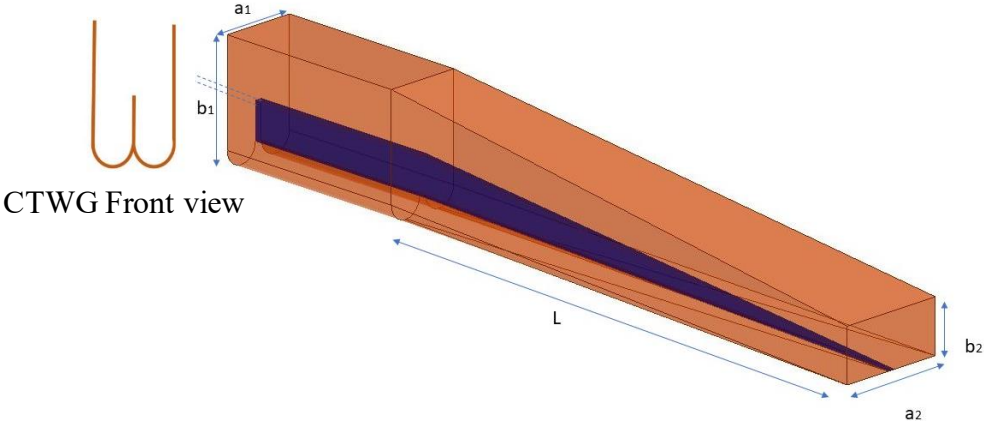**Figure 21: RWG mode to CTWG mode conversion and impedance transformation.**

Figure 22: RWG to CTWG transition having tapered septum.

Utilizing the same design procedure, a CWG to TWG transition has been designed as shown in figure 22. The dimension of the circular waveguide is same as that of standard

30

medium size V-band circular waveguide diameter. The transition is of length L and diameter d on one end and the other end has the same dimension as the one designed in RWG – CTWG transition. The septum thickness is uniform along the length of the transition. The side walls of the transition merge to the side walls of troughguide in a curved manner, maintaining the decrease in overall horizontal width.
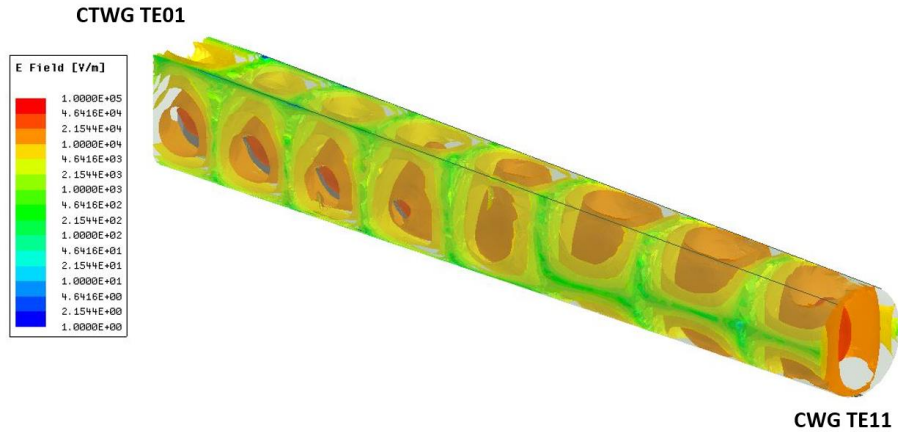
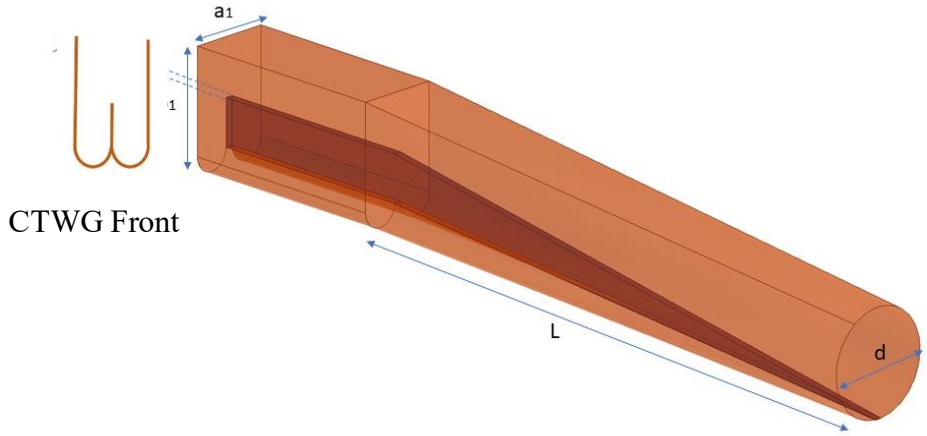**Figure 23: CWG mode to CTWG mode conversion and impedance transformation.**

Figure 24: CWG to CTWG transition having tapered septum.

III.3 Mode Conversion and cutoff wavelength

The transition length and cutoff frequency depends on the principal mode in consideration and the taper profile used in design. Stepped and linear taper implemented in [15] provides us a starting point in the design of transition acting as a dual-polarizer rotator. We need to ensure that impedance transformation and mode conversion is being achieved with the dimension in our control. The RWG TE01 mode has a cutoff wavelength which decides the dimension of RWG.

Similarly, the cut-off for TWG is determined by keeping the base width less than half the cutoff-wavelength set at 1.1mm. This is done to avoid any field variation along the width of the TWG. Finite septum thickness of 0.25mm is considered with a septum height of 1.65mm. With these restrictions on the various dimensions of the design, we can control the impedance and mode conversion changing the length L and the taper profile. The TWG is viewed as a closed structure having a magnetic wall slightly above the septum with an electric wall at the center of the troughguide along the height of the septum. This electric wall has a central null along the vertical axis which divides the guide into two sections. Therefore, the mode analysis can be done same as that for any RWG. The characteristic impedance for each is Zo respectively and 2Zo for the TWG as it appears in series on the narrow wall.
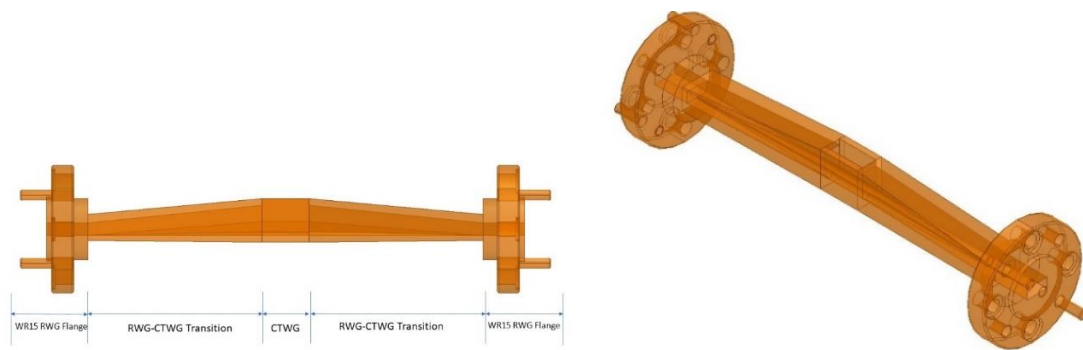
Figure 25: Back to back transition having RWG and Unit Cell of CTWG.
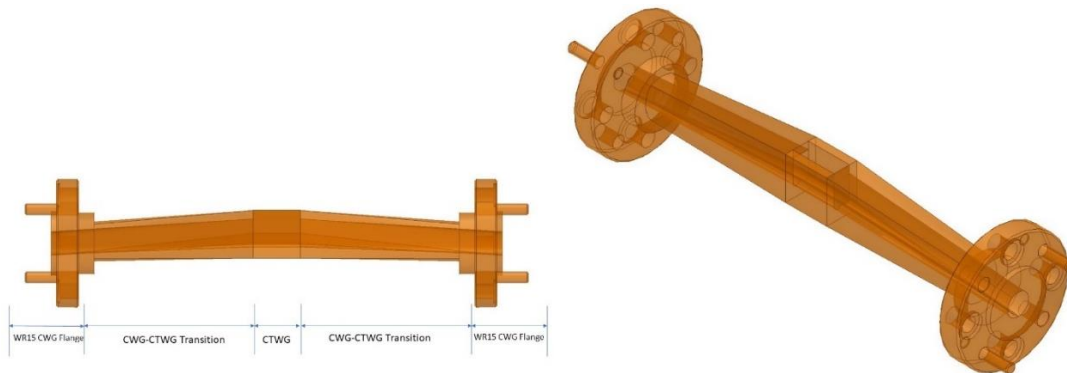

Figure 26: Back to back transition having CWG and Unit Cell of CTWG.

A linear tapering has been utilized to realize the required mode conversion and the impedance is approximated based on the cutoff of RWG and equivalent RWG derived from the dimensions of each TWG section.

Figure 27 shows the variation in VSWR with variation in the length of the transition which enables us to finalize an optimum required length. Based on simulated results an RWG-CTWG with length of 30mm and a CWG-CTWG with a length of 26mm has been fabricated.
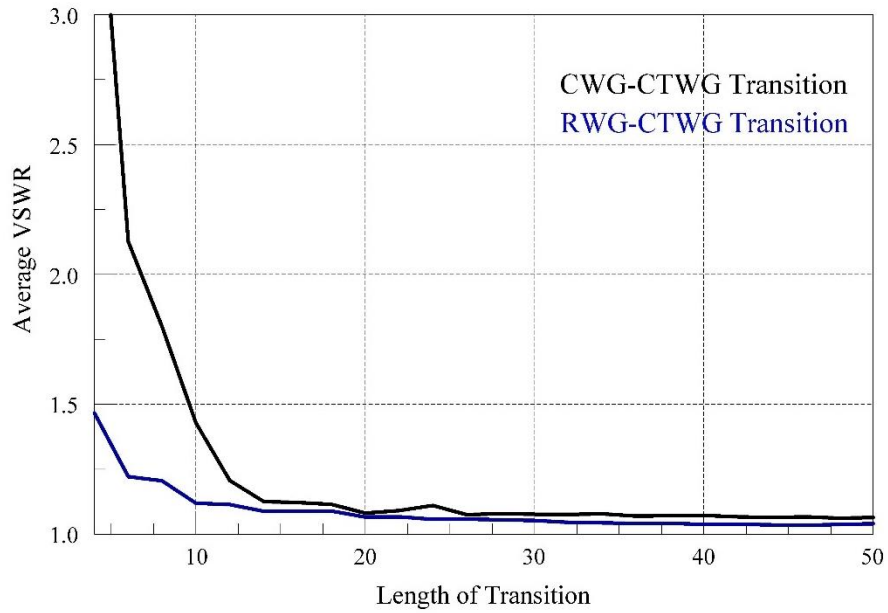
Figure 27: Average VSWR w.r.t to the Length of Transition.

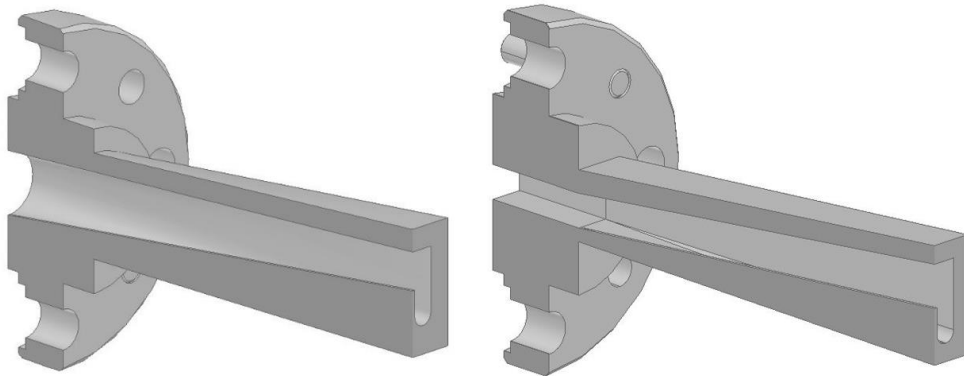### III.4 Fabricated Model and Test Setup

Figure 28: Section of CAD models for Transitions.

Initial design and simulation have been conducted using HFSS [17] EM tool to accomplish the results and working of the designed transitions. RWG to CTWG transition

34

shown in Fig.25 and a CWG to CTWG transition has been designed and simulated as shown in Fig. 26. The Transition is connected in a back to back configuration with a unit cell of troughguide in between the two. Standard Flanges have been used with dimensions same as that used in Coaxial to waveguide adapters commercially. This is to ensure there are no error in the measured results due to Flange mismatch. An RWG -CWG converter was used between both the ports of VNA for testing the CWG-CTWG transition. The converter and the TRL kit used for calibration was designed using the fabrication process discussed in the previous chapter. The overall setup utilized for performing the measurements includes a back to back transition with UG385/U flanges, two RWG-CWG converters having U flange on one end and UG383/U-M flange, 1.85mm to WR15 RWG adapters, low loss cables and a VNA shown in Figure 29.
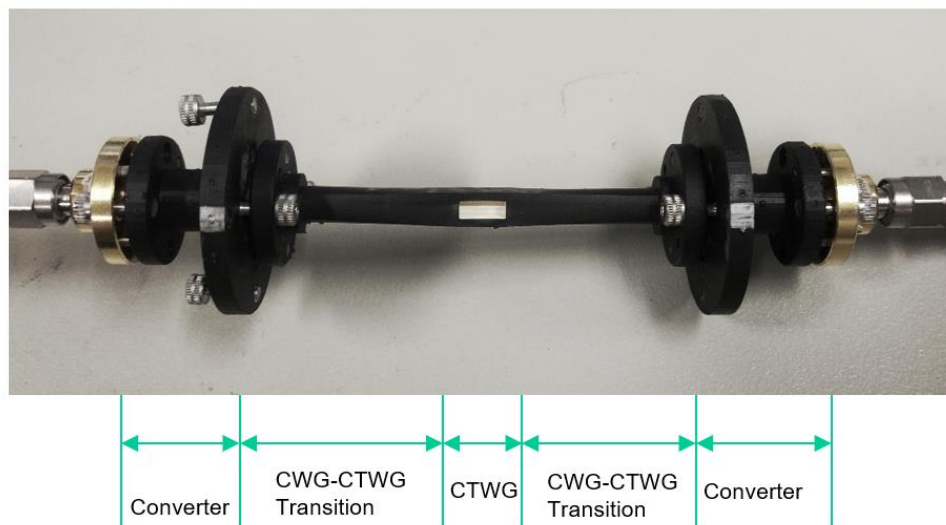

Figure 29: Testing Setup used to Measure S-parameters.

III.5 Simulation and Measurement Results

The measurement results for the fabricated RWG-CTWG transition having an insertion loss of about -0.4 to -0.7dB is close to the value of -0.26dB analyzed in the simulations, Figure 30. The return loss between the two port is less than -18 dB for the entire range of desired frequency as seen in Figure 31.
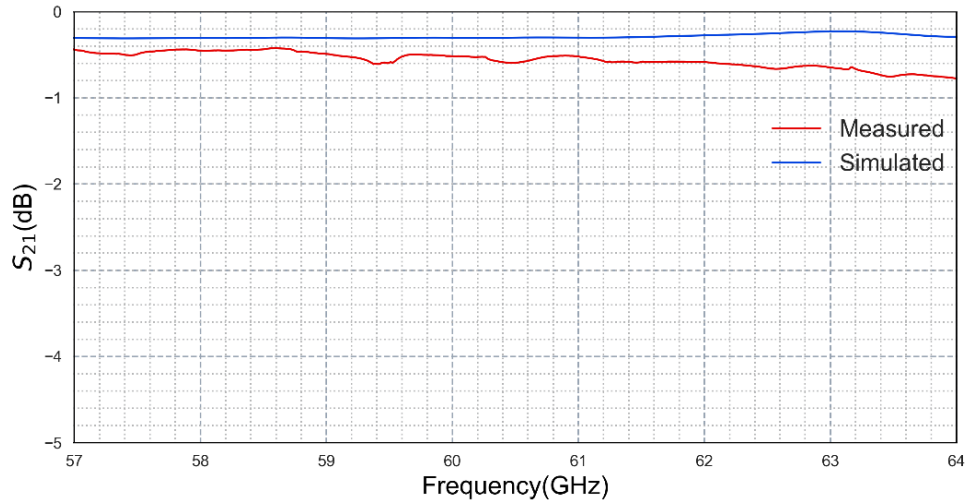

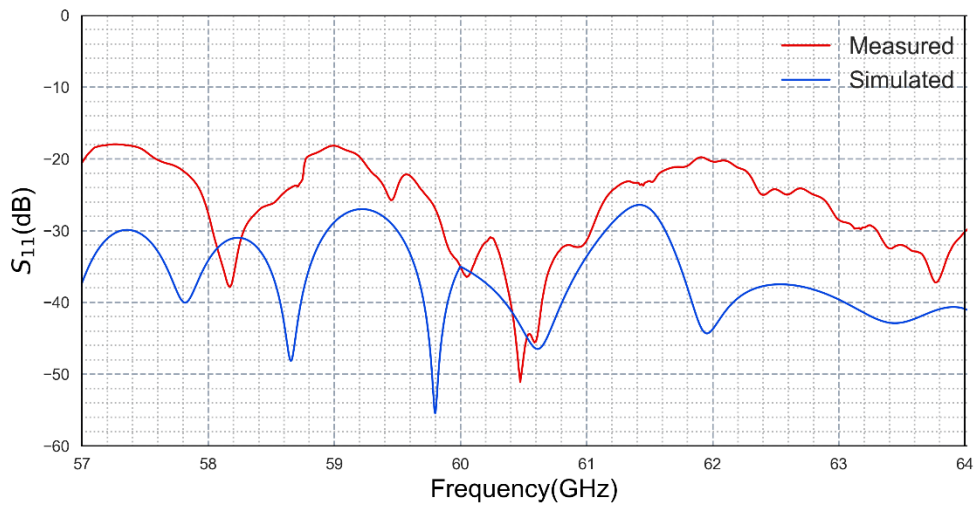**Figure 30: Insertion Loss of the RWG-CTWG B2B Transition.**

Figure 31: Reflection Loss of the RWG-CTWG B2B Transition.

Similar results have been achieved for the CWG-CTWG transition having values of insertion loss and return loss close to the simulated results as seen from the plots in Figure 32 and 33.
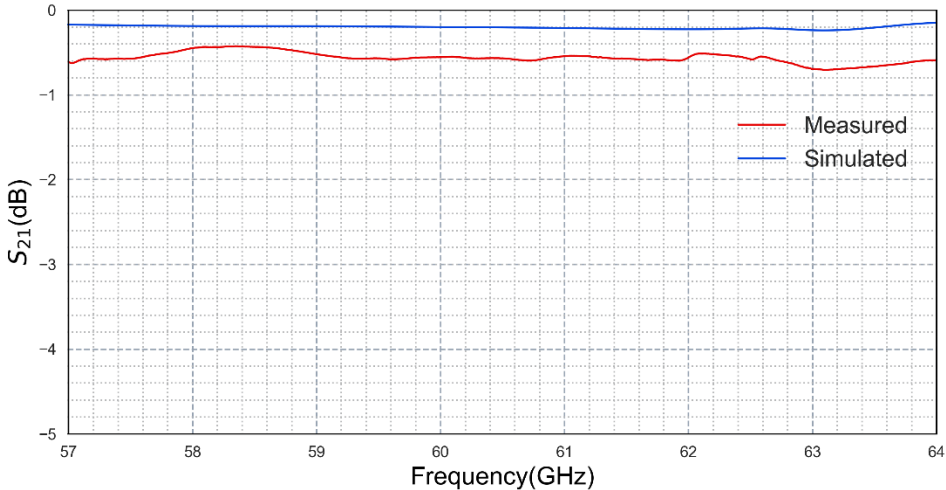

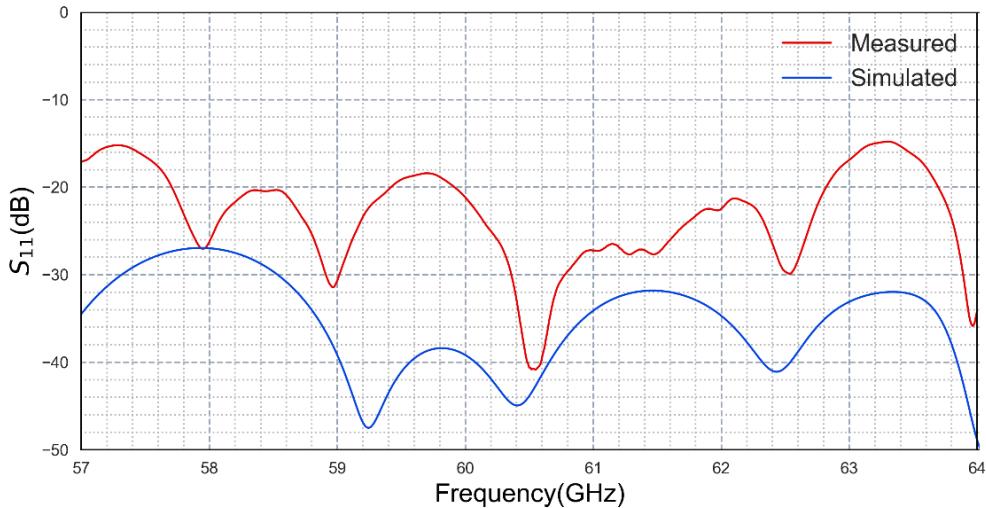**Figure 32: Insertion Loss of the CWG-CTWG B2B Transition.**

Figure 33: Reflection Loss of the CWG-CTWG B2B Transition.

CHAPTER IV

TROUGH WAVEGUIDE ANTENNA

IV.1 Introduction

Troughguide with continuous asymmetry or periodic asymmetry has been used to attain phase accumulation and phase reversal in a way that the principal mode radiates energy from the open end. There are some techniques for creating a radiating waveguide with the use of horizontal and vertical tuning rods and mode coupling radiating rods. The technique involves using discrete radiator of either resonant or non-resonant elements. First part of this chapter attempts at using perturbations of half wavelength alternately placed on each side of the guide called as periodically asymmetric TWA. A comparison has been made between a rectangular TWA and the circular TWA having same number of elements and of the same size. S-parameters, radiation pattern and matching has been analyzed. Second part talks about various matching techniques utilized to reduce impedance mismatch that occurs for a broadside radiation pattern.

IV.2 TWA without matching

Asymmetric TWA having resonant blocks placed periodically along the length for a rectangular TWA has been designed first. Each perturbation is alternately placed on each side of the guide to create a unit cell. 16 such unit cell has been repeated throughout the guide for creating a linear array of resonant elements. The length of each base block is fixed at half guide wavelength in order to achieve a phase reversal of 180 degrees at each interface. The guide wavelength is kept less than twice the free space wavelength, to

ensure only one principal beam in the broadside direction. The angle of this beam is given by equation E. Setting the angle at 0 degrees, value for required length of the perturbations can be verified which is equal to the guide wavelength.
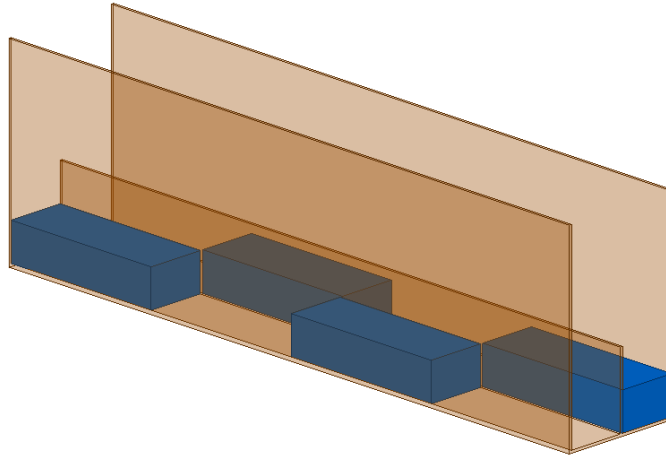

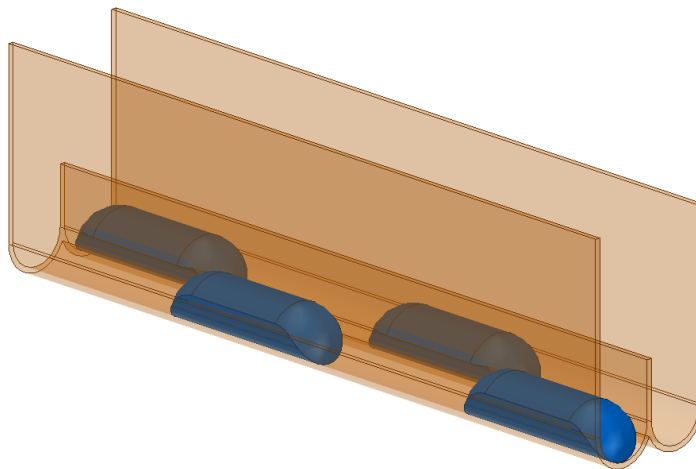**Figure 34: TWA with Rectangular blocks as perturbations.**

Figure 35: TWA with antipodal perturbations.

Considering the rectangular Troughguide antenna as a starting point for designing it at 60 GHz, certain modifications has been made. The rectangular blocks used as

perturbations has been changed into an antipodal structure to avoid any sharp edges seen in Figure 35. Sharp edges and narrow spacing between to surface inside the waveguide cause abrupt junction between the two, which in turn affects the expected results. These modifications help us in fabricating the antenna with minimum viable thickness and smooth edges. The better approach is to account these modifications and attain desired results beforehand. Fluid flow utilized for plating the inner walls of the guide is also considered in the final design. The perturbations appear to have a tapered shaped on both the edges along its length, which fuses into the base of the troughguide. Figure 35 shows the designed Circular TWA with transitions attached on both the ports.
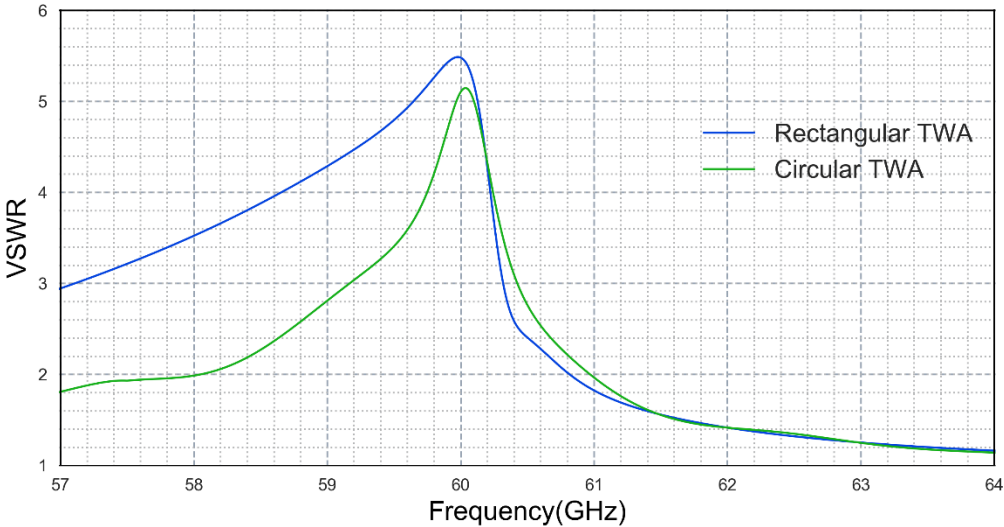

Figure 36: Simulated results for two Troughguide antenna.

The value of VSWR peaks at 60GHz where the value of reflections due to impedance mismatch is maximum. The wave gets attenuated as seen from plot, the value of reflection loss is around -3.5dB which is very high due to the reflections accumulated at each interface. Since both the designs have values close to each other, it proves that the

design with circular base and antipodal perturbations can be used for creating a matched troughguide antenna. These results are compared in the Figure 37 and 38.
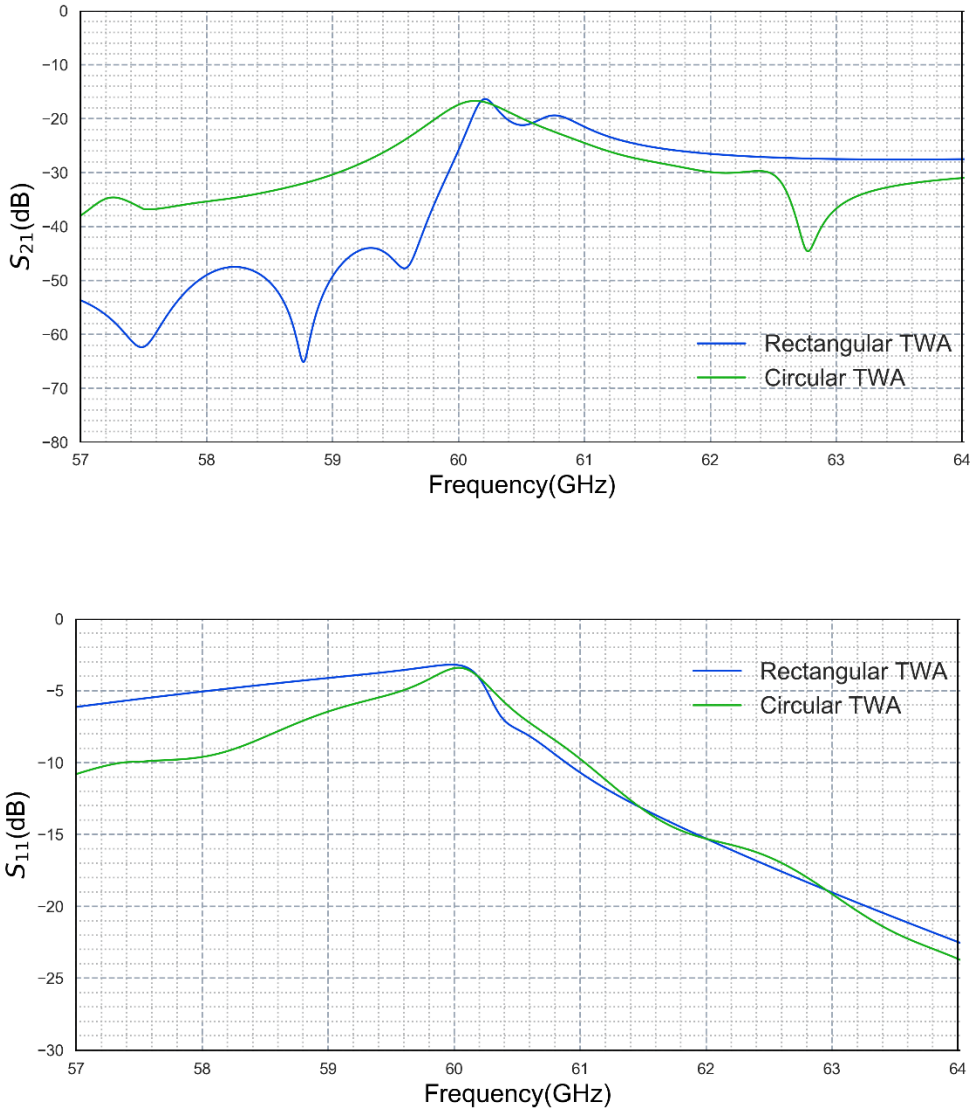

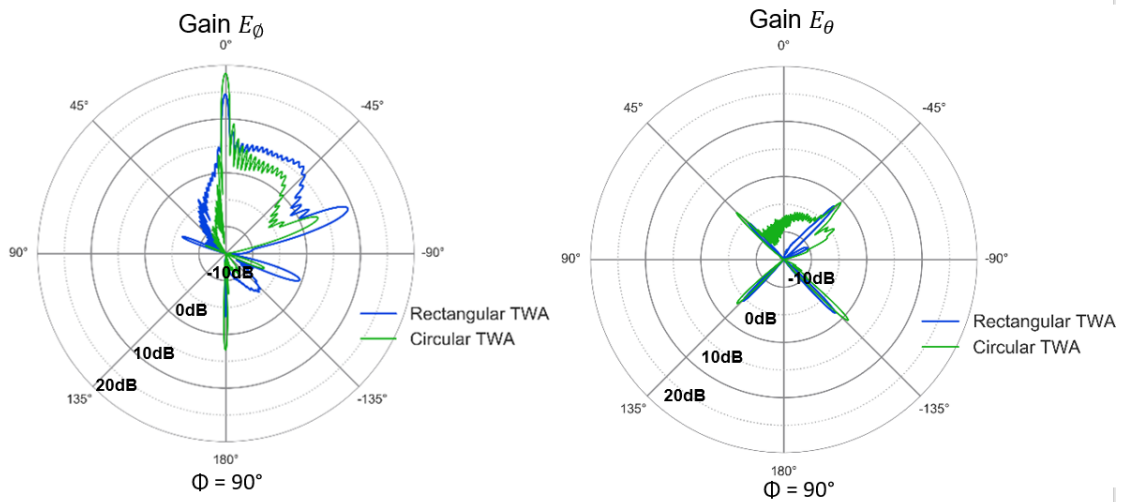**Figure 37: S-parameter for Troughguide antenna.**

Figure 38: Co-polarization and cross-polarization plane radiation pattern.

The radiation pattern for the circular TWA shows a reduction in the sidelobes as the perturbations have a smooth rounded edge causing a slight tapering. Also, there is an increase in the directivity of the antenna in the broadside region.

IV.3 Circular TWA with rectangular blocks matching
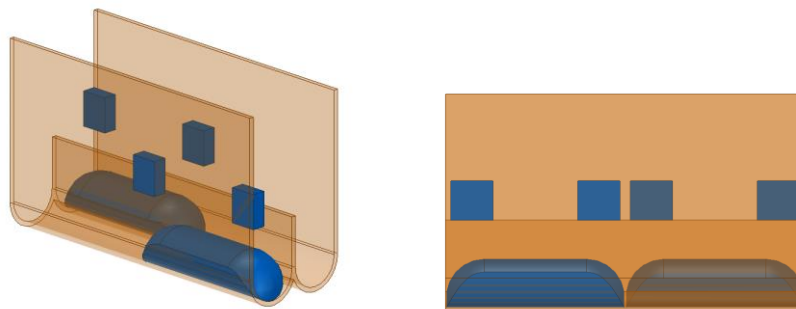

Figure 39: Rectangular matching posts.

Previous work on impedance matching trough waveguide antenna makes use of tuning posts placed on the septum. This has been done using non-resonant tuning posts on

the septum and on the side walls of the troughguide. Considering the finite size of septum for a design at 60GHz, it becomes tough to use the same idea for adding tuning posts. Since the thickness of the septum is about 250 microns, it will be a strenuous task to fabricate the antenna with the desired dimensions and achieve the required results at the same time. The perturbations placed along the waveguide creating reflections at the interface appearing as a shunt negative susceptance without any matching. These reflections can be matched by placing a capacitive tuning post along the side walls at each of these interfaces. Considering the symmetry of design, the antenna has two ports either of which can be excited with other port being terminated with appropriate matched impedance. A rectangular post has been added for initial confirmation of matching attained as shown in figure 39. The equivalent circuit for the perturbation and the tuning posts has been shown in figure 40 and 41. The tuning posts can be viewed as a window formed by an obstacle of finite thickness where the edges are perpendicular to the E field.
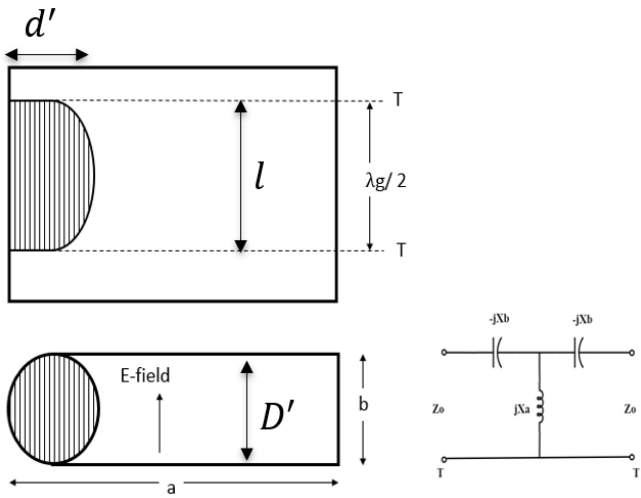
D' and D_1 are the dimensions of perturbation.

Figure 40: Equivalent circuit model for perturbations in CTWG.

43

Following equations (56)-(59) are used to determine the values of reactance in the equivalent circuit [18]:

$$\frac{X_a}{Z_0} = \frac{4b}{\lambda_g}\left(\frac{b}{\pi D\prime}\right)^2, \quad \frac{\pi D\prime}{\lambda} \ll 1 \tag{56}$$

$$\frac{X_b}{Z_0} = \frac{b}{16\lambda_g}\left(\frac{\pi D_1}{b}\right)^4, \quad \frac{\pi D_1}{\lambda} \ll 1 \tag{57}$$

$$D\prime = \sqrt{\frac{d\prime(l+d\prime)}{2}} \tag{58}$$

$$D\prime = \left(\frac{ld\prime(l+d\prime)^2}{2}\right)^{1/4} \tag{59}$$

l is the length and $d\prime$ is the height of the perturbations. X_a and X_b are the equivalent reactance and Z_0 is the characteristic impedance of the RWG created on one side of the troughguide.
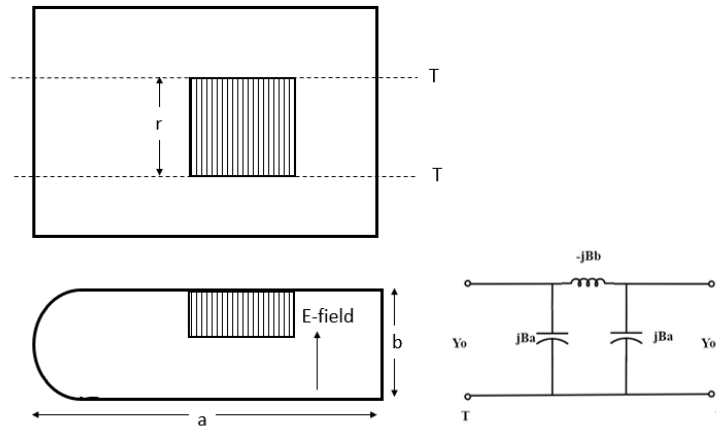

Figure 41: Equivalent circuit model for rectangular posts in CTWG.
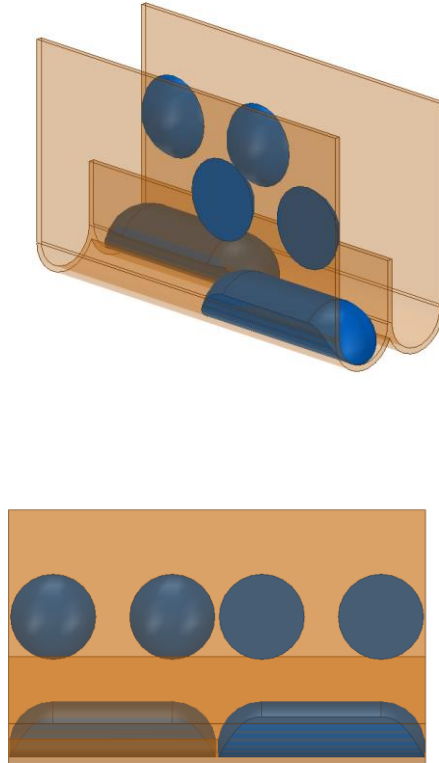
44

IV.4 CTWA with spherical matching

Figure 42: Spherical matching posts.

The rectangular tuning post proves the theory of matching each interface for the impedance mismatches at the resonant frequency. The sharp edges and corners result in a non-uniform plating of metal on the surface as the contact made by Tollen's reagent is not laminar. Therefore, a spherical tuning post has been utilized to attain the same results as before. After removing the sharp edges and corner, there is slight increase in the VSWR which has been accounted in the final design.

The equivalent circuit shown in figure 43 for spherical post remains same as that for rectangular with a slight change in the values of circuit components. The tuning post is viewed as a window formed by an obstacle with elliptical cross section.
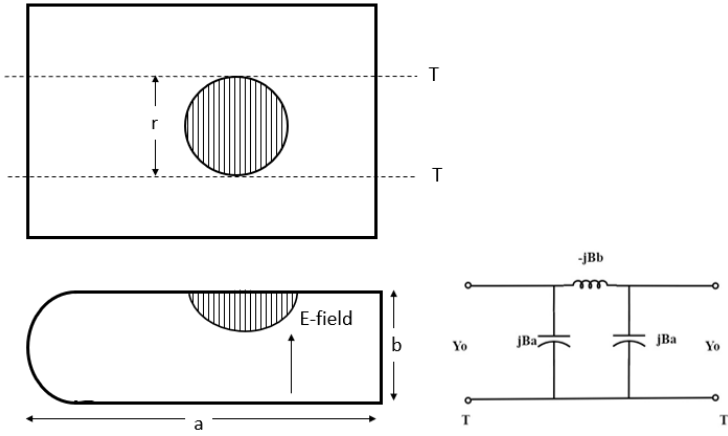

Figure 43: Equivalent circuit model for spherical posts in CTWG.

Following are the simulation results for TWA with two different shapes of the matching elements shown in Figure 44-46:
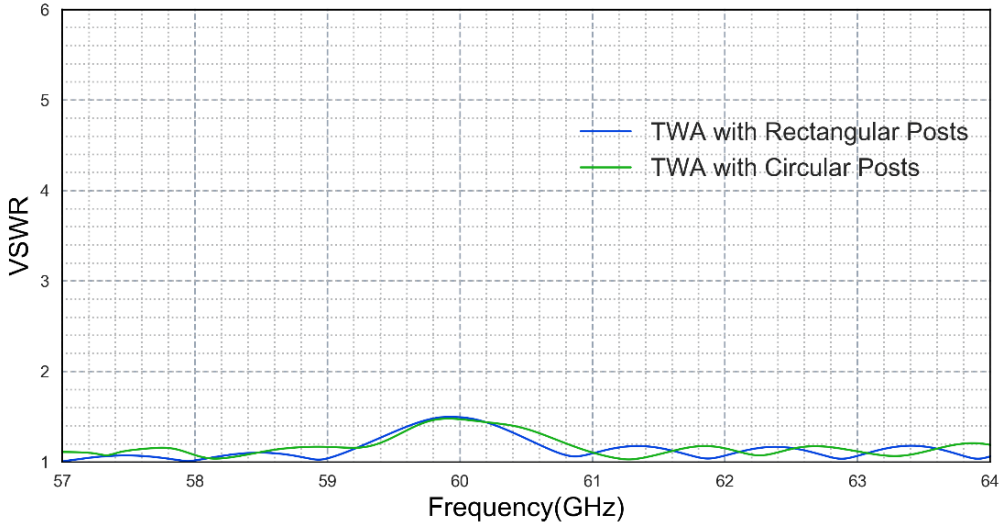

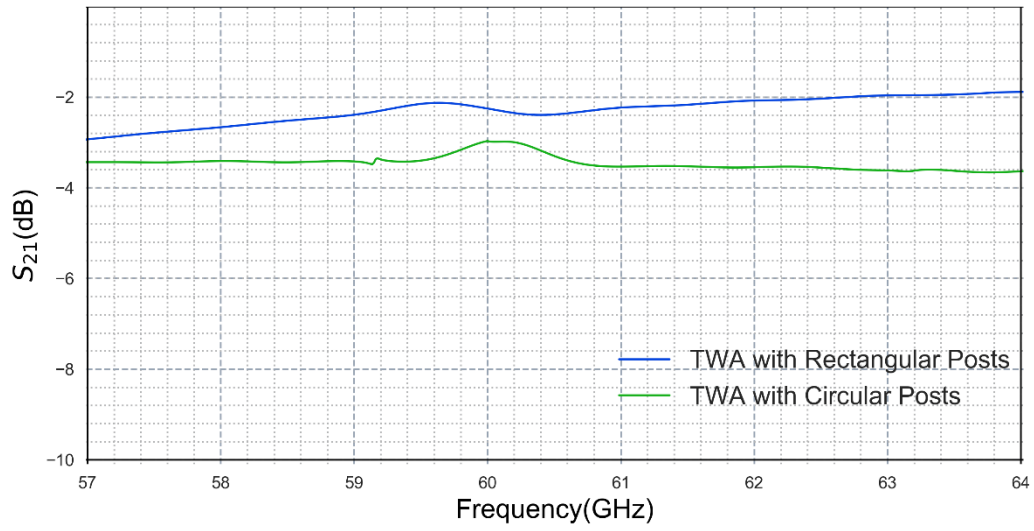**Figure 44: VSWR for TWA with Rectangular and Circular matching elements.**

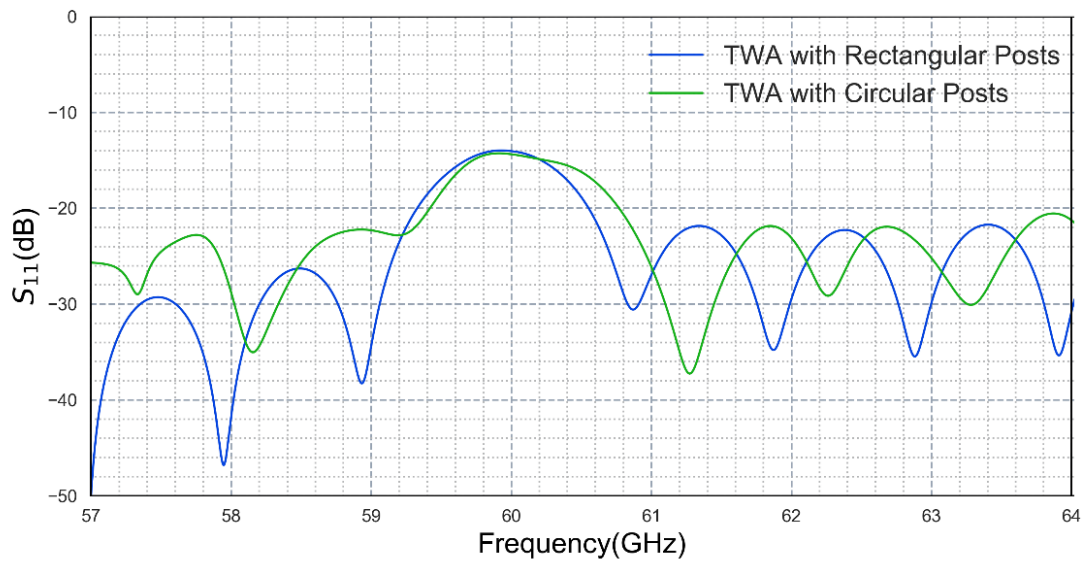**Figure 45: Insertion Loss for Troughguide antenna.**

Figure 46: Reflection loss for Troughguide antenna.

47

The radiation pattern obtained for the antenna having rectangular mathcing elements is shown in figure 47. The pattern obatined after modifying the rectangular element into a spherical element appears to be close to the previous design.
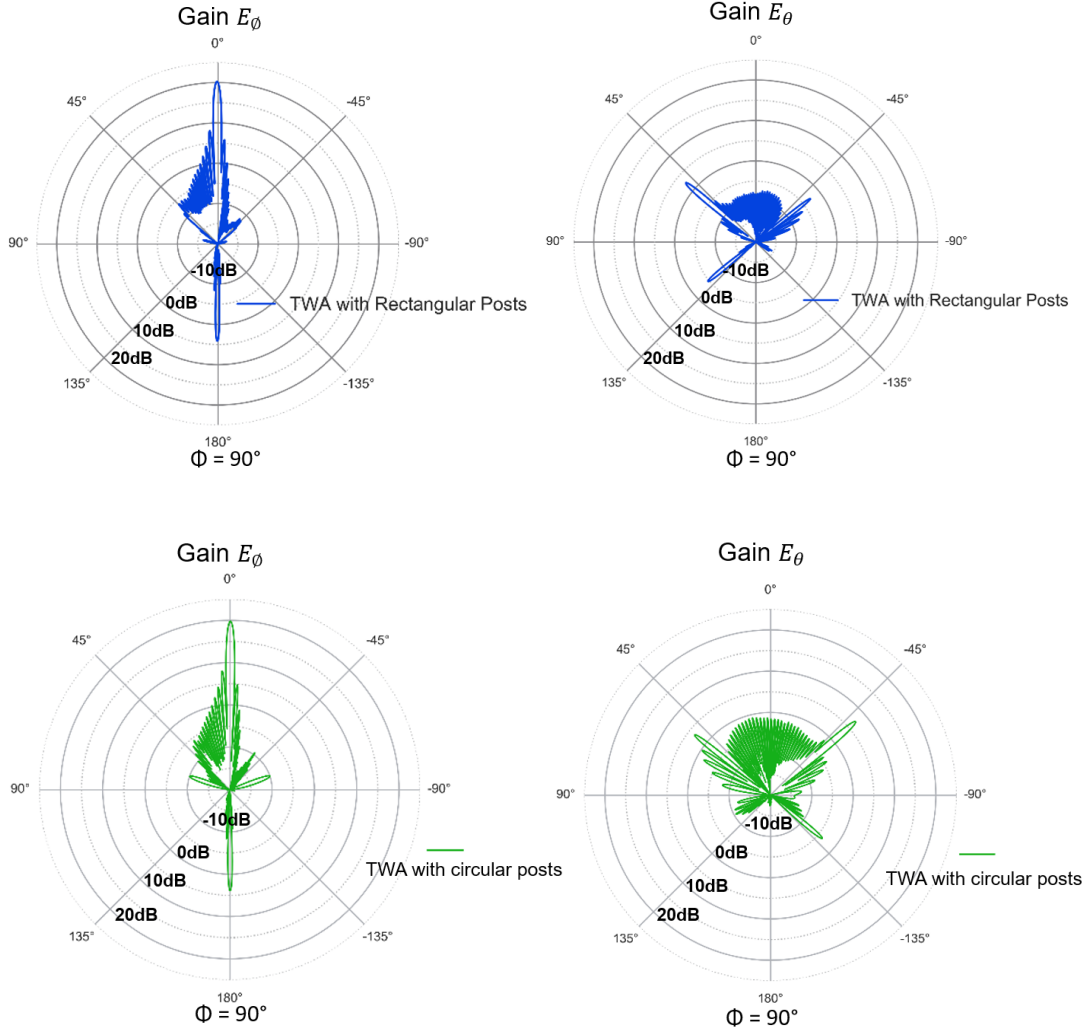

Figure 47: Radiation pattern for Troughguide antenna with rectangular and circular posts.

IV.5 Results

The complete design is shown in the Figures 48-50, starting from the CAD model and step by step process of fabrication.
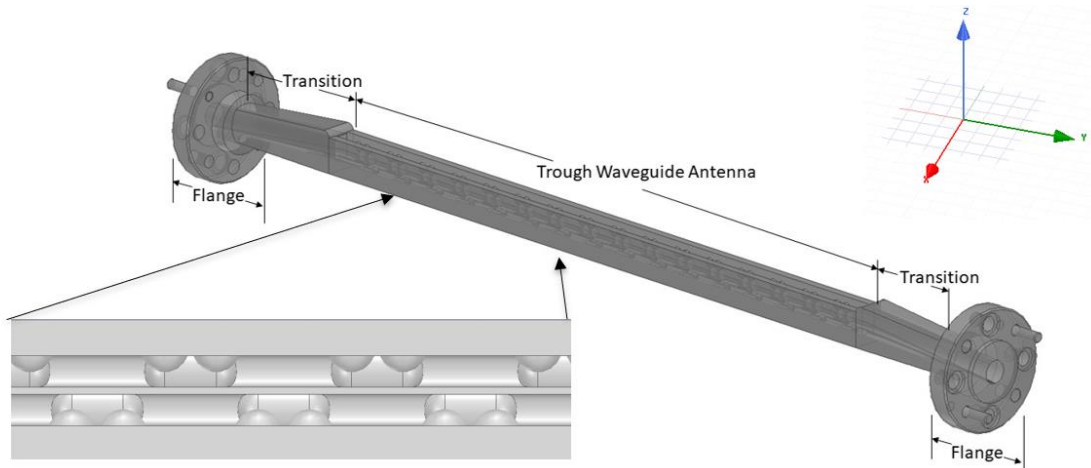

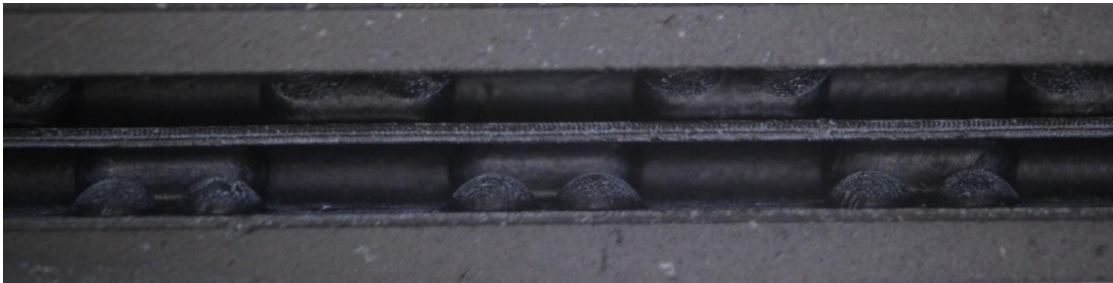
Figure 48: CAD model for TWA with matching elements.

Figure 49: 3D Printed model for TWA with matching elements.

Figure 50: Plated model for TWA with matching elements.
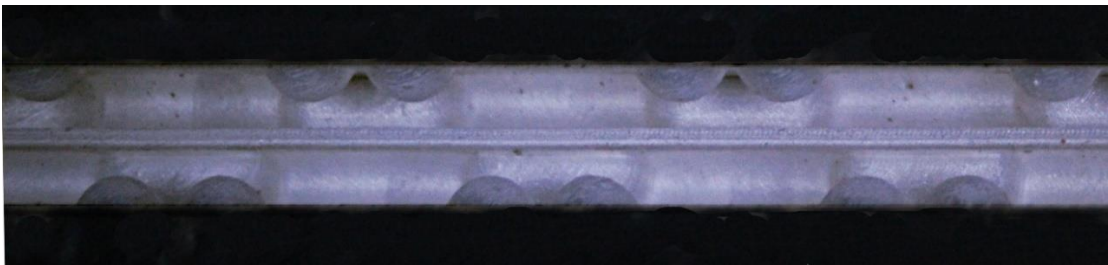
The measured results show an increase in the operating frequency due to the tolerances in fabrication process. Average value of return loss and insertion loss for the measurements is close to the expected values.
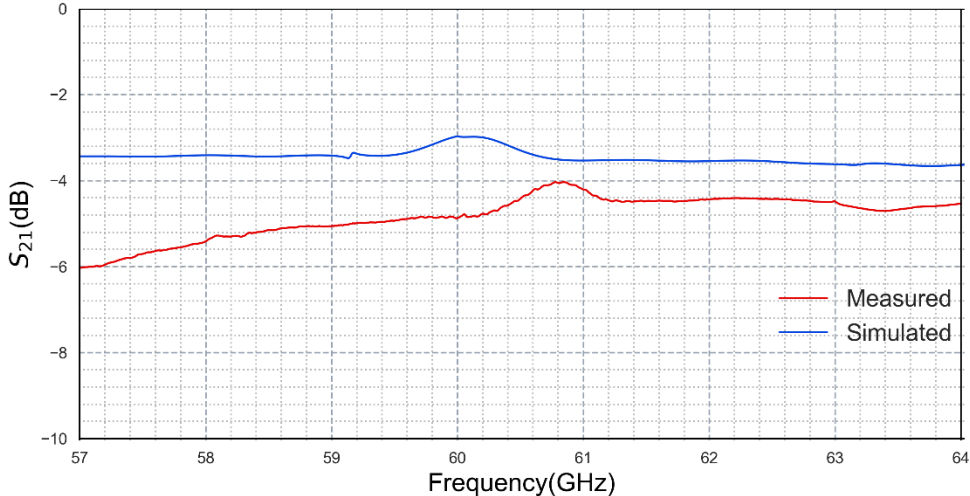
Figure 51: Measured and Simulated Insertion Loss for Troughguide antenna.
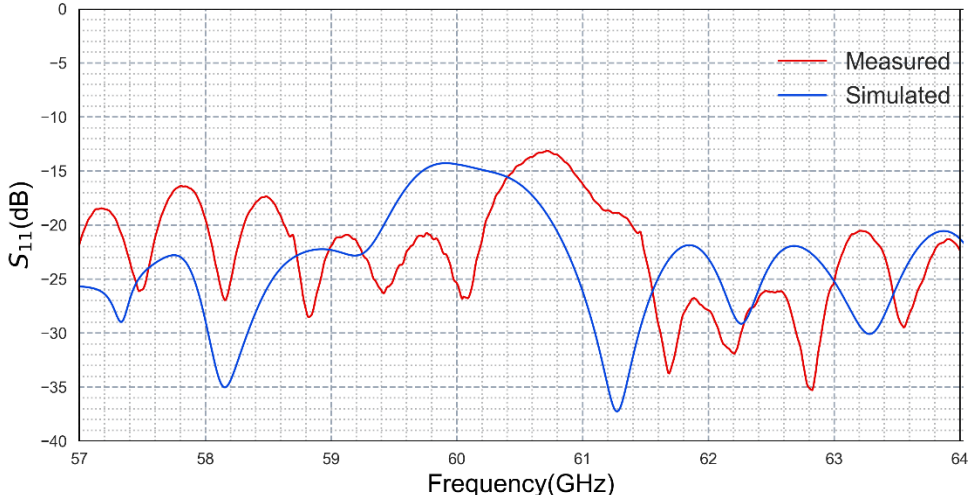
Figure 52: Measured and Simulated Reflection Loss for Troughguide antenna.

Figure 53: Measured and Simulated VSWR for Troughguide antenna.

The radiation pattern in Figure 54 shows a reduction in the sidelobes and an increase in the peak gain. The matching elements can couple energy from the dominant mode and radiate it out from the open end providing a matching at the same time.

Figure 54: Simulated radiation pattern for Troughguide antenna.

CHAPTER V

FREQUENCY SCANNING OF BEAM AND AMPLITUDE TAPER
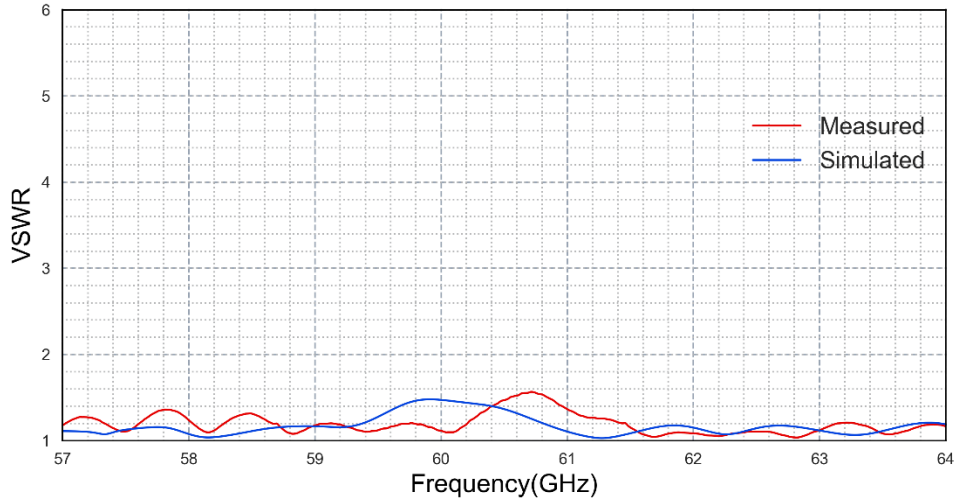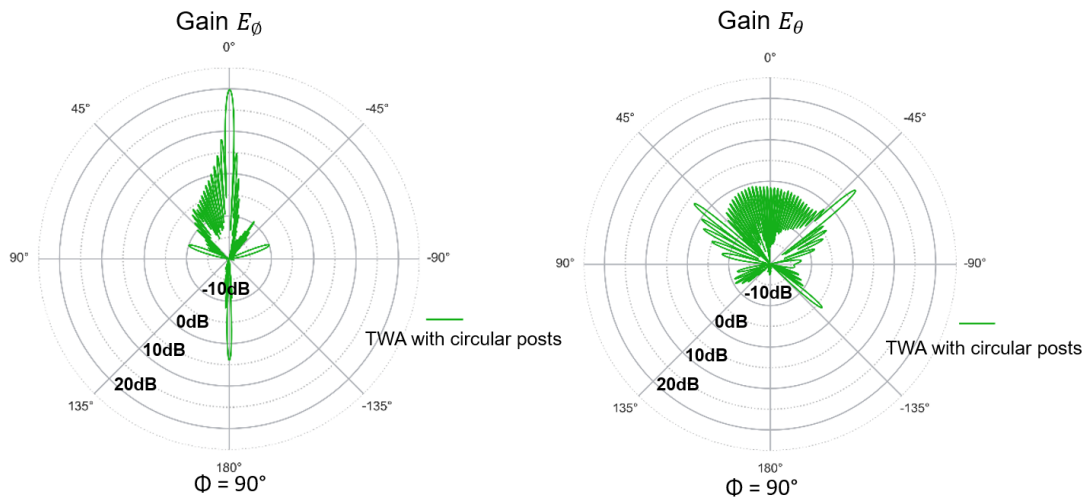
Many applications such as Radar require a narrow beam with high directivity able to scan a certain angle along the direction in which a target traverse. This scanning can be achieved by either varying the source excitation frequency or a variation in the phase for an antenna array. The change in frequency is achieved by using a variable frequency oscillator able to sweep the frequency in the desired band.

Radiation pattern and reflection parameters for the Trough waveguide antenna designed in the previous section has been analyzed in this chapter. The source has been swept from 57Ghz to 64Ghz at 1Ghz step. A shift of 1.5 degrees is achieved in each step of 1 GHz around the broadside direction of antenna orientation for co-polarization plane as viewed in Figure 55.
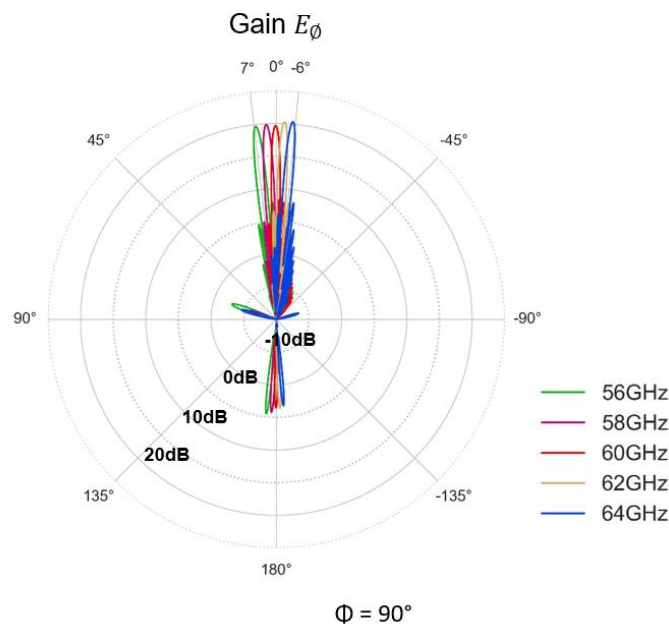

Figure 55: Frequency scanning of main beam in Troughguide antenna.

V.1 Amplitude tapering

The current distribution along the transmission line affects the width of beam for a radiation pattern. Depending on the variation of current the height of side lobes can be minimized [19], [20]. Various taper profiles such as Triangular, Cosine and squared cosine have been derived to attain a certain value of normalized side lobe level. For an unmatched TWA having all the perturbation of equal height, a large amount of power is radiated in near endfire and near broadside direction. These are the side lobes which can be reduced by applying an amplitude tapering to the perturbations. The height of each perturbation can be adjusted using the calculated taper distribution to attain the desired pattern.
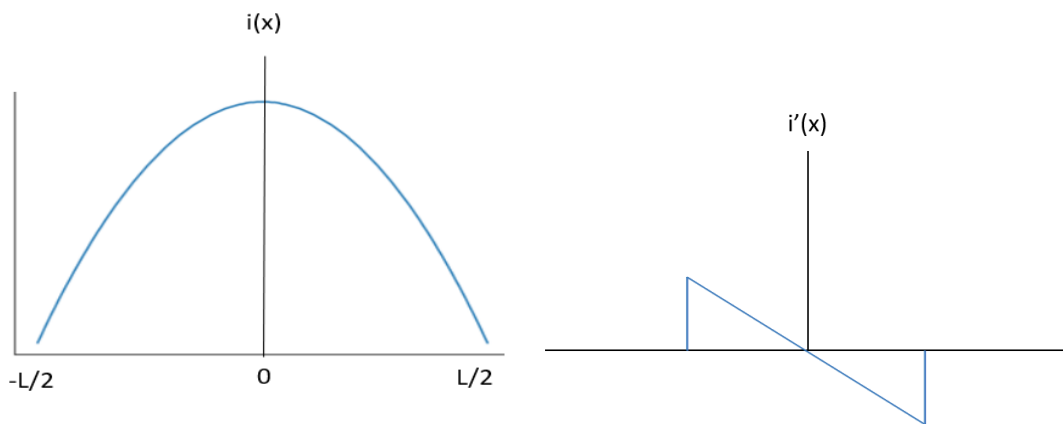

Figure 56: Aperture excitation and First derivative.

A parabolic taper has been implemented having the amplitude distribution for the aperture excitation as shown in figure 56. The first and the second derivative is plotted for the aperture length where the second derivative appears as impulses with constant

amplitude at the edges. The far-field radiation pattern with a reduction in sidelobes by a value of -22dB has been calculated.
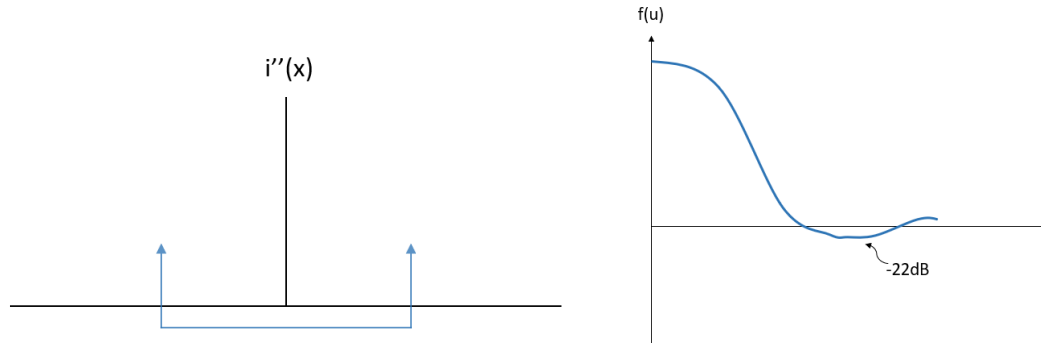
Figure 57: Second derivative and Far-field radiation pattern.

The trough waveguide antenna with symmetrically tapered perturbation is designed as shown if figure 58. The vertical arrows denote the change in perturbation height along the waveguide length, maximum at the center and minimum at the input and output ports.

Figure 58: Amplitude taper using variation in perturbation height.

As seen in the below result, there is a significant reduction in the sidelobe level around near-endfire and near-broadside regions.
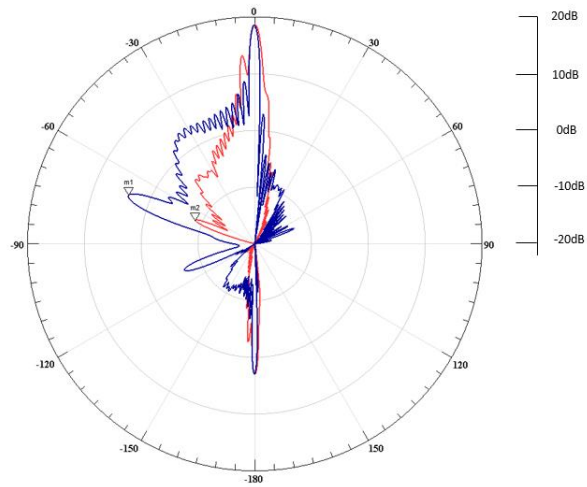
Figure 59: Radiation Pattern for tapered and non-tapered TWA.

CHAPTER VI

FUTURE WORK

Impedance matching and amplitude tapering has been discussed in this thesis with establishes the theory minimizing the return loss and lowering the sidelobes. Maximizing the radiation efficiency of the TWA is one of the 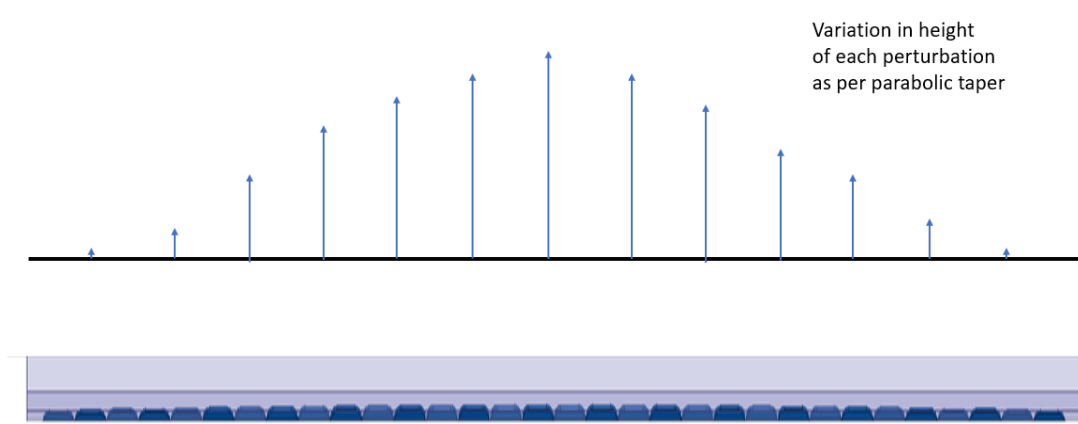important aspects that needs consideration in the future iterations of the design. An array of such antenna with multiple input and output ports will be created to apply progressive phase shift for beam scanning applications. The overall radiation pattern can be controlled in the required manner based on the suitable amplitude tapering window.

Reconfiguration of the antenna can be achieved using liquid metal flowing into the channels created beneath the perturbations. Also, the waveguide can be filled with dielectric material to provide mechanical support and cover the open end of the waveguide.

CHAPTER VII

CONCLUSION

Fabrication of RWG/CWG to CTWG transitions using additive manufactured materials and electroless plating were discussed in the thesis which shows close approximation with the simulated and measured results. Impedance matching techniques for the reflections caused at the operating frequency to attain broadside pattern has been established. Design modifications required for fabricating the septum, perturbations and the tuning elements has been discussed achieving the same results as that for designs without modifications.

Tapering of the perturbations to further reduce the sidelobes has been discussed utilizing various standard taper profiles. Significant amount of reduction has been obtained in the sidelobes for the unmatched TWA.

REFERENCES

[1]   D. M. Pozar, "Microwave Engineering", 3th ed., New York, *John Wiley & Sons, Inc*, 2005, pp. 116-140

[2]   R. Harrington, "Time-Harmonic Electromagnetic Fields", New York, *Wiley-IEEE Press*, 2001, pp. 212-234

[3]   R. Collin, "Field Theory of Guided Waves", New York, *Wiley-IEEE Press*, 1990, pp. 51-56

[4]   R. Paknys and D. R. Jackson, "The relation between creeping waves, leaky waves, and surface waves", *IEEE Transactions on Antennas and Propagation*, vol. 53, no. 3, March 2005, pp. 898-907.

[5]   W. Rotman and N. Karas, "Some new microwave antenna designs based on the trough waveguide," in *IRE International Convention Record*, 1956, pp. 230-235, 1956

[6]   W. Rotman and A. A. Oliner, "Periodic structures in trough waveguide," *IRE Transactions on Microwave Theory and Techniques,* vol. 7, 1959, pp. 134-142.

[7]   W. Rotman and A. Oliner, "Asymmetrical trough waveguide antennas," *IRE Transactions on Antennas and Propagation,* vol. 7, 1959, pp. 153-162.

[8]   W. Rotman and A. Maestri, "An electromechanically scannable trough waveguide array," in *IRE International Convention Record*, 1960, pp. 67-83.

[9]   D'Auria, M., Otter, W. J., Hazell, J., Gillatt, B. T. W., et al, "3-D printed metal-pipe rectangular waveguides," *IEEE Transactions on Components, Packaging and Manufacturing Technology*, vol. 5, 2015, pp. 1339-1349.

[10] Le, S. and Gregory, P., "3D printed waveguide slot array antennas," *IEEE Access, vol. 4*, 2016, pp. 1258-1265.

[11] Shen, J., Aiken, M., Ladd, C., Dickey, M. D., Ricketts. D. S., "A simple electroless plating solution for 3D printed microwave components," *Microwave Conference (APMC), Asia-Pacific, IEEE*, 2016, pp. 1-4.

[12] Bal, A., Carey, D.G., Espinal, F. A. and Huff, G. H., "Electroless silver plating of 3D printed waveguide components by peristaltic pump driven system*,"* *Electronics Letters*, vol. 55(2), 2018, pp. 100-102.

[13] G. D. Hopkins, B. K. Edenfield, J. G. Hampton and R. L. Roberts, "A new coax to troughguide transition," *IEEE Microwave and Wireless Components Letters,* vol. 12, 2002, pp. 299-301.

[14] G. H. Huff and A. S. Long, "Reconfigurable radiation from a W-band trough waveguide antenna: trade-offs in impedance and radiation from tapered MEMS based perturbations," in *Proc. of the IEEE Antennas and Propagation Society International Symposium,* 2007, pp. 109-112.

[15] K S Packard, "The Cutoff Wavelength of Trough Waveguide", *Airborne Instruments Lab, Correspondence*, 1958, pp. 455-456.

[16] C. M. Rappaport and F. R. Morgenthaler, "Localized hyperthermia with electromagnetic arrays and the leaky-wave troughguide applicator," *IEEE Transactions on, Microwave Theory and Techniques,* vol. 34, 1986, pp. 636-643.

[17] Ansys Electronics Desktop V19.1 Module HFSS: Ansoft corporation, Pittsburgh, PA 15219, http://www.ansoft.com/products/hf/hfss/.

[18]   M. V. Andreev, O. O. Drobakhin, A. L. Makarov and V. O. Sydoruk, "Reduction of the side-lobe level of the radiation pattern of the multielement linear radiator based on a trough waveguide," *2017 XXIInd International Seminar/Workshop on Direct and Inverse Problems of Electromagnetic and Acoustic Wave Theory (DIPED)*, Dnipro, 2017, pp. 217-220.

[19]   N. Marcuvitz, Waveguide Handbook, MIT Rad. Lab. Ser. (Vol 10), *McGraw-Hill*, 1951, pp. 353-355.

[20]   R. Elliott, Antenna Theory & Design: New York, *Wiley-IEEE Press*, 2003, pp. 98-122.

[21]   S. Hopfer, "The design of ridged waveguides," *IRE Transactions on Microwave Theory and Techniques*, vol. 3, 1955, pp. 20-29.

[22]   K H Yeap, C Y Tham, G Yassin, K C Yeong, "Attenuation in Rectangular Waveguides with Finite Conductivity Walls", *Radio Engineering*, vol. 20(2), 2011, pp. 472-478.